Electronic Supplementary Information

Design of Salt-Metal Organic Frameworks Composites for Seasonal Heat Storage Applications†

Anastasia Permyakova,[a,b] Sujing Wang,[a] Emilie Courbon,[b] Farid Nouar,[a,c] Nicolas Heymans,[b] Pierre D'Ans,[d] Nicolas Barrier,[e] Pierre Billemont,[b] Guy De Weireld,[b] Nathalie Steunou,[a*] Marc Frère[b*] and Christian Serre [a,c]

[a.] *Institut Lavoisier, UMR CNRS 8180, Université de Versailles St-Quentin en Yvelines, 45 Avenue des Etats-Unis, 78035 Versailles Cedex, Université Paris-Saclay, France. E-mail : nathalie.steunou@uvsq.fr*

[b.] *Institut de Recherche en Energie, Service de Thermodynamique et de Physique mathématique, Université de Mons, Boulevard Dolez 31, B-7000 Mons, Belgique. E-mail : marc.frere@umons.ac.be*

[c.] *Institut des Matériaux Poreux de Paris, FRE 2000 CNRS, Ecole Normale Supérieure, Ecole Supérieure de Physique et des Chimie Industrielles de Paris, PSL Research University, 75005 Paris, France. E-mail : christian.serre@ens.fr*

[d.] *4MAT Department, Université libre de Bruxelles (ULB), 50 Avenue F.D. Roosevelt- CP 194/3, B-1050 Bruxelles, Belgium*

[e] Laboratoire CRISMAT, CNRS UMR 6508, 6 bvd Maréchal Juin, 14050 CAEN CEDEX, France

I. Thermochemical energy storage

Thermochemical energy storage is based on reversible exo-/endothermic reaction of storage material with working fluid (generally, water). Adsorption process (zeolite, silica gel) or hydration process (salt) which is activated by bringing the dry storage material in contact with a working fluid results in release of heat energy. The seasonal space heating applications imply energy charging in summer period and heat release (energy discharging process) in winter. The Figure S1 shows the scheme of closed-system device for seasonal heat storage.

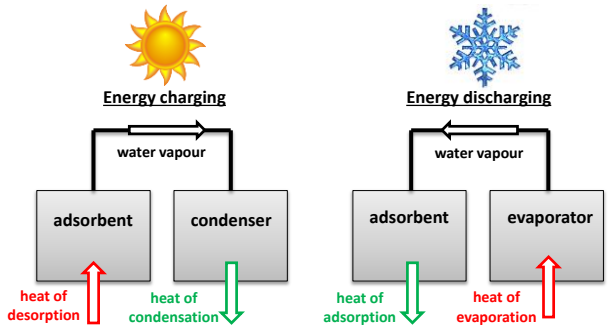

Figure S1. Closed-system device for seasonal heat storage

II. Water sorption experiments

The cycling loading lift under cycle boundary condition (p=12.5 mbar, T_a=30°C, T_d=80°C) was carried out using an Intelligent Gravimetric Analyzer (IGASorp Moisture Sorption Analyzer) or thermogravimetric analyzer (TG-DSC111) connected with generator of humidity Setaram. The IGASorp allows to precisely control the water vapor pressure (1-95 RH% with an accuracy of ± 0.1% RH) and temperature (5-80°C with an accuracy of ±0.1°C). Prior to the analysis, samples were dried for 12 h under N_2 flow at the same temperature as for N_2 sorption measurements for each sample. At first adsorption isotherm was carried out at temperature 30°C and R.H. range 5-50% with step of 5% (the point at R.H. 30% corresponds to p=12.5 mbar). Then the sample was treated by dry N_2 at 30°C before being submitted to an isotherm measurement at 80°C and R.H. range of 2.6-7.8% with step of 3% (the point at R.H. 2.6% corresponds to p=12.5 mbar). It is noteworthy, that desorption at 80°C was performed on material without complete drying (only by dry N_2 at 30°C) in order to correspond to the real conditions in the reactor. The exchanged mass of water between adsorption at 30°C and desorption at 80°C at 12.5 mbar was considered as cycling loading lift.

The cycling loading lift under cycle boundary condition (p=12.5 mbar, T_a=30°C, T_d=80°C) and multiple cycles of water adsorption-desorption were carried out using a thermogravimetric analyzer (TG-DSC111) connected with generator of humidity Setaram with RH stability of ± 0.3%. The sample was first dried for 12h under vacuum at the same temperature as for N_2 sorption measurements for each sample. Nitrogen gas flow was firstly humidified (T=40°C, RH=17.4%) and then was passed through thermogravimetric balance. The adsorption profiles were collected at 30°C in humid nitrogen at 12.5 mbar until equilibrium (during 48 hours). The desorption step were performed at 80 °C at 12.5 mbar until equilibrium (during 48 hours).
The adsorption heat measurements were done on Setaram TG/DSC111 connected to Setaram Wetsys humidity generator system. Nitrogen was used as inert gas. The flow rate of humid gas was 30 mL/min. Prior to analyses samples were dried under vacuum during 10 hours at 150°C for UiO-66(Zr)-NH_2, MIL-125(Ti)-NH_2 and at 180°C for MIL-127(Fe). The sample was then cooled down to 30°C under vacuum. The adsorption step was then measured at 30°C and 1.25 kPa (humidity generator at 40°C and relative humidity RH=17.4%). The integration of the heat flow signal using the horizontal last point integration mode gives the heat of adsorption expressed in J/g of MOF.

III. Characterization of MOFs

1. X-ray powder diffraction

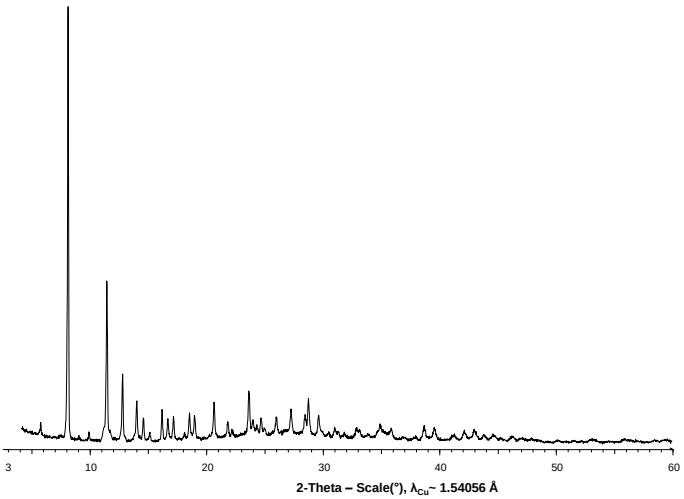

Figure S2. PXRD pattern of MIL-127(Fe) in 2Θ range 4-60° (step 0.02°, 17 s per step)

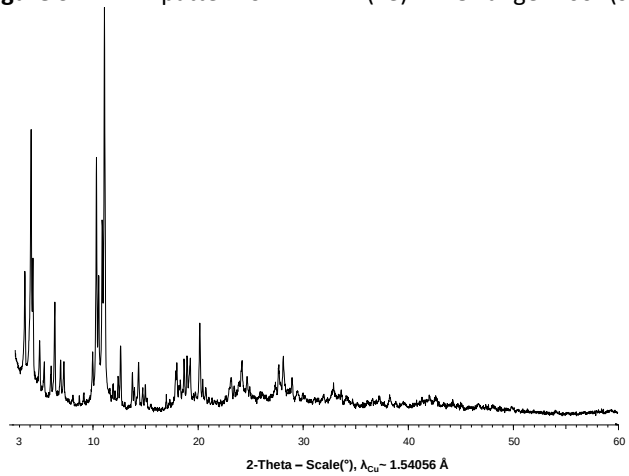

Figure S3. PXRD pattern of MIL-100(Fe) in 2Θ range 2.5-60° (step 0.02°, 17 s per step)

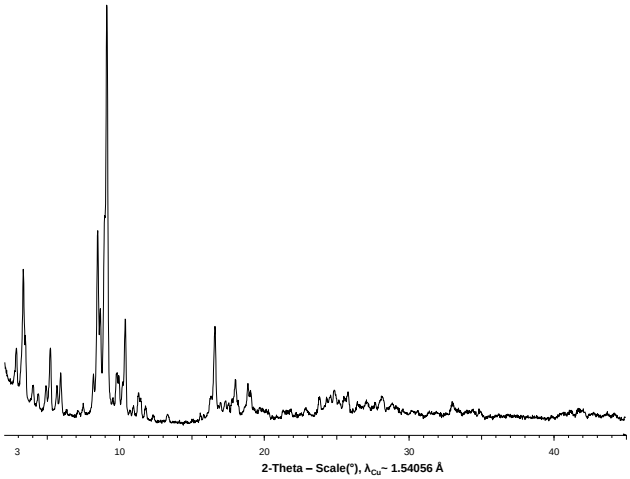

Figure S4. PXRD pattern of MIL-101(Cr) in 2Θ range 2-45° (step 0.02°, 17 s per step)

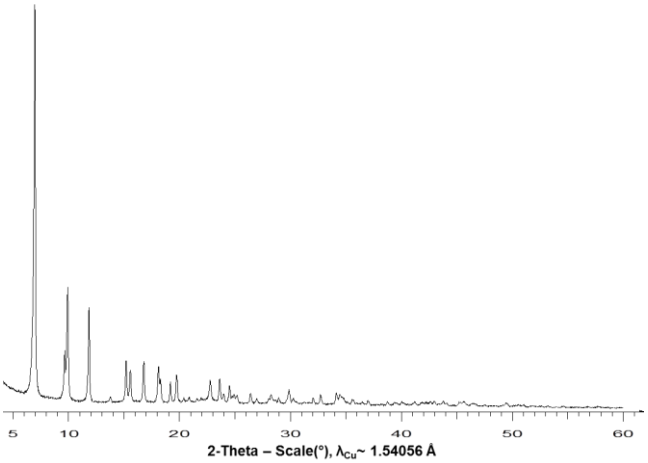

Figure S5. PXRD pattern of MIL-125(Ti)-NH_2 in 2Θ range 4-60° (step 0.02°, 17 s per step)

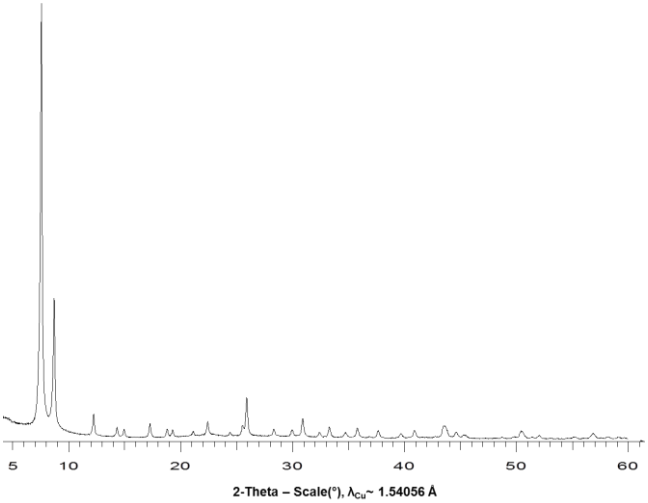

Figure S6. PXRD pattern of UIO-66(Zr)-NH_2 in 2Θ range 4-60° (step 0.02°, 17 s per step)

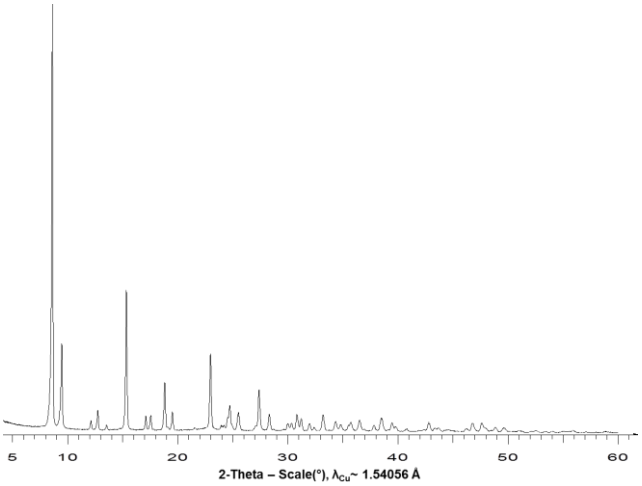

Figure S7. PXRD pattern of MIL-160(Al) in 2Θ range 4-60° (step 0.02°, 17 s per step)

2. Thermogravimetric analysis

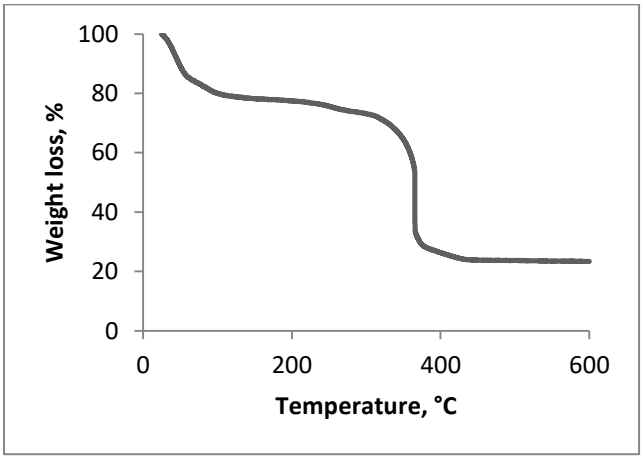

Figure S8. Thermogravimetric analysis profile of MIL-127(Fe) under oxygen flow (carrier gas flow rate: 200 ml/min).

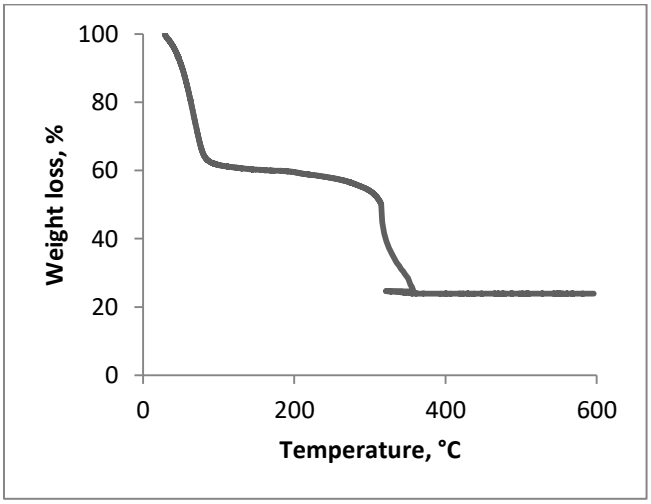

Figure S9. Thermogravimetric analysis profile of MIL-100(Fe) under oxygen flow (carrier gas flow rate: 200 ml/min).

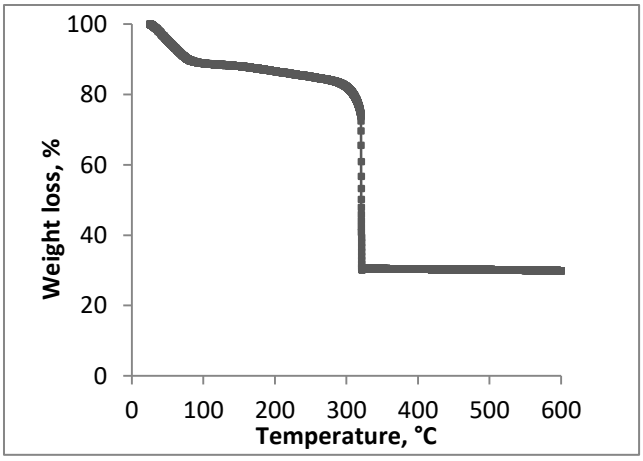

Figure S10. Thermogravimetric analysis profile of MIL-101(Cr) under oxygen flow (carrier gas flow rate: 200 ml/min).

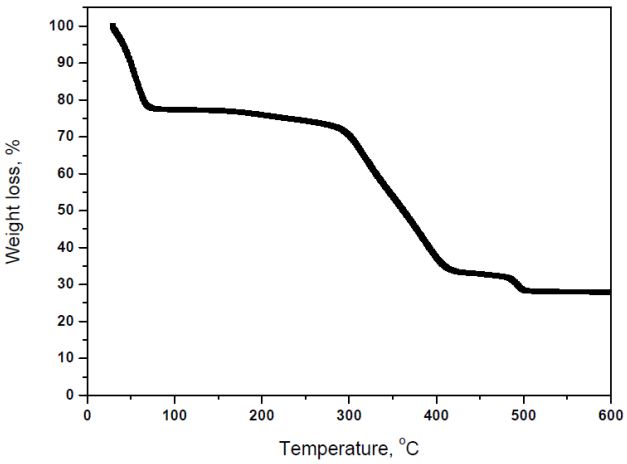

Figure S11. Thermogravimetric analysis profile of MIL-125(Ti)-NH_2 under oxygen flow (carrier gas flow rate: 200 ml/min).

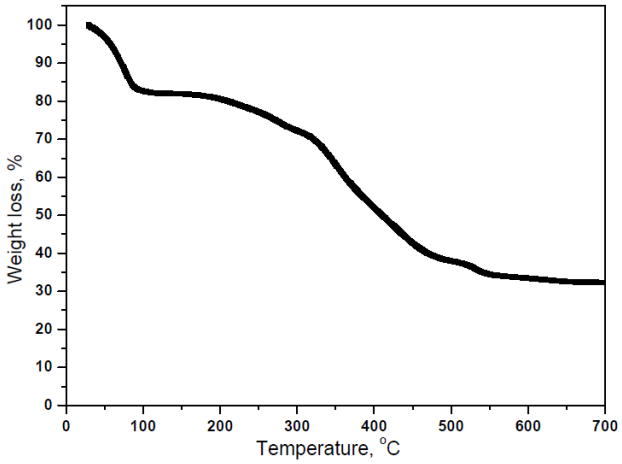

Figure S12. Thermogravimetric analysis profile of UIO-66(Zr)-NH_2 under oxygen flow (carrier gas flow rate: 200 ml/min).

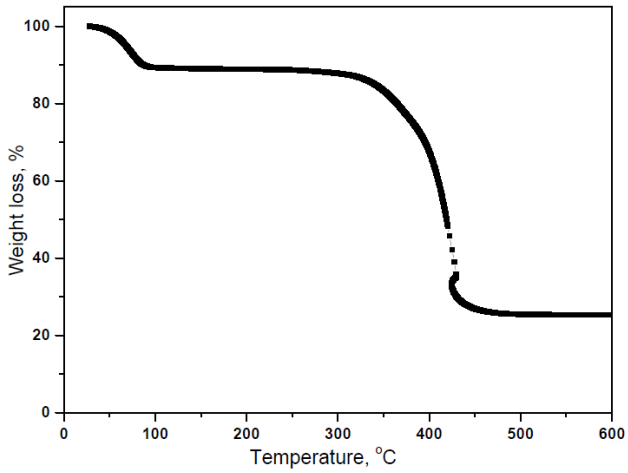

Figure S13. Thermogravimetric analysis profile of MIL-160 under oxygen flow (carrier gas flow rate: 200 ml/min).

3. N_2 sorption porosimetry

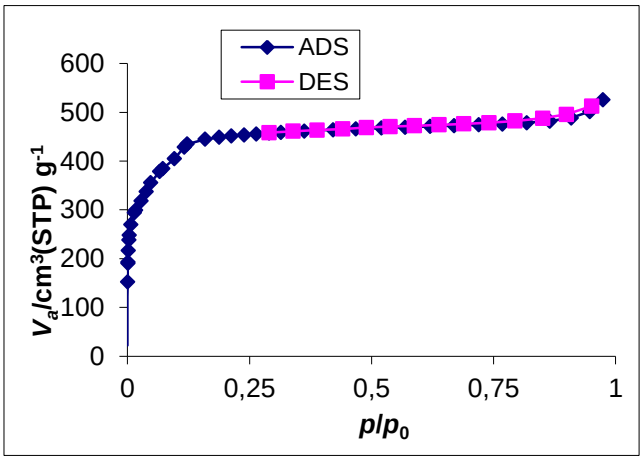

Figure S14. Nitrogen sorption isotherm of MIL-100(Fe) at 77 K (S_{BET} = 1828 m^2/g, V_{pore} = 0.81 cm^3/g). Temperature of pretreatment is 180°C.

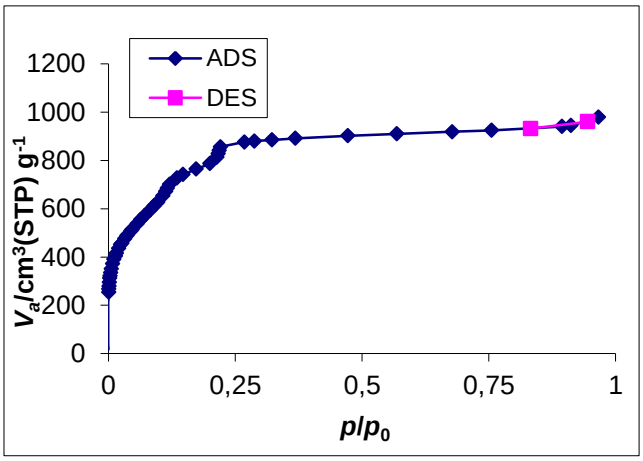

Figure S15. Nitrogen sorption isotherm of MIL-101(Cr) at 77 K (S_{BET} = 3721 m^2/g, V_{pore} =1.51 cm^3/g). Temperature of pretreatment is 200°C.

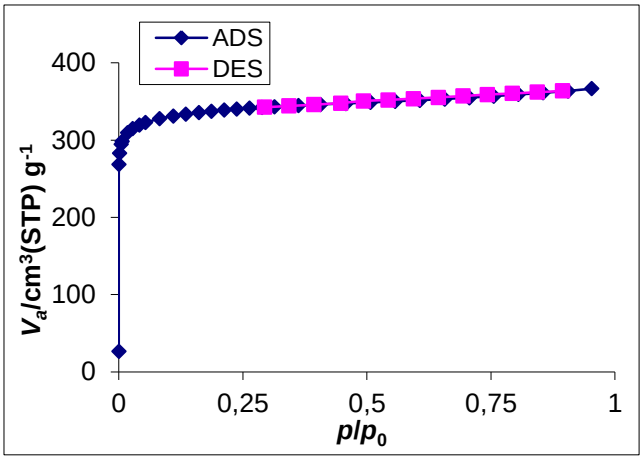

Figure S16. Nitrogen sorption isotherm of MIL-127(Fe) at 77 K (S_{BET} = 1342 m^2/g, V_{pore} =0.57 cm^3/g). Temperature of pretreatment is 180°C.

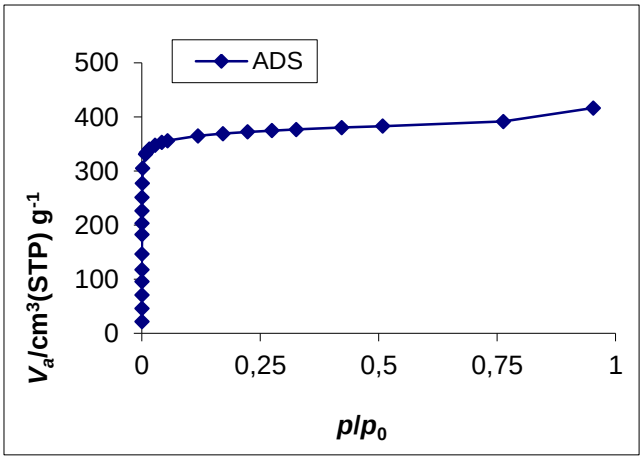

Figure S17. Nitrogen sorption isotherm of MIL-125(Ti)-NH_2 at 77 K (S_{BET} = 1450 m^2/g, V_{pore} =0.64 cm^3/g). Temperature of pretreatment is 180°C.

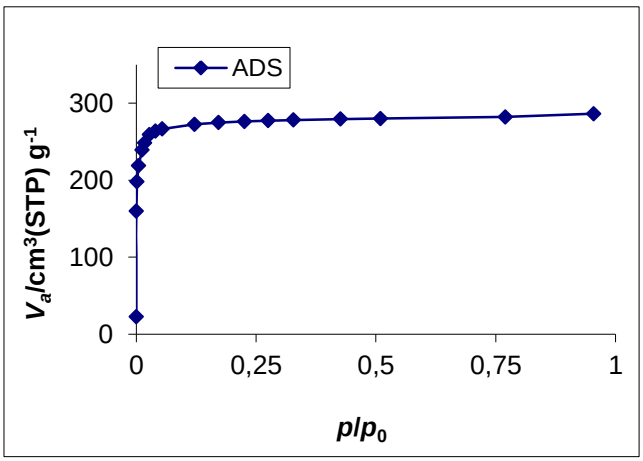

Figure S18. Nitrogen sorption isotherm of UiO-66(Zr)-NH_2 at 77 K (S_{BET} = 1119 m^2/g, V_{pore} =0.44 cm^3/g). Temperature of pretreatment is 150°C.

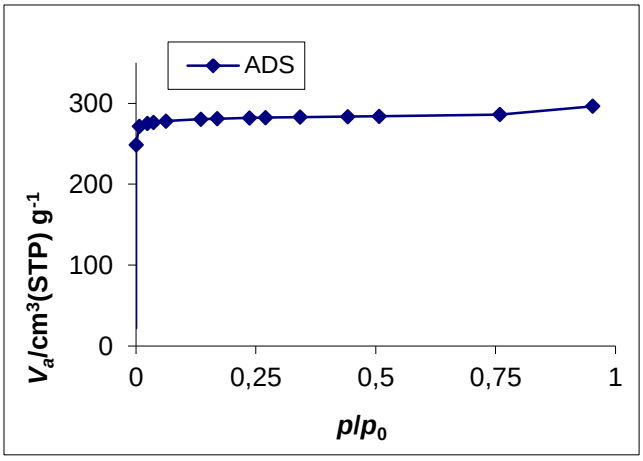

Figure S19. Nitrogen sorption isotherm of MIL-160 at 77 K (S_{BET} = 1148 m^2/g, V_{pore} =0.46 cm^3/g). Temperature of pretreatment is 150°C.

4. Water sorption of MOFs

The achievable cycle loading lift (g water/ g dry material) is the working fluid exchange between the production cycle (adsorption) and the regeneration cycle (desorption). As mentioned above (ESI II) information about cycling loading lift under boundary conditions could be obtained by two devices: IGASorp and TG-DSC coupled to humidity generator. Figure S20 summarizes the adsorption loading lift (T=30°C, p=12.5 mbar) and cycling loading lift (between T=30°C and T=80°C, p=12.5 mbar) of MIL-101(Cr), MIL-127(Fe), MIL-100(Fe), UiO-66(Zr)-NH_2, MIL-125(Ti)-NH_2, MIL-160(Al).

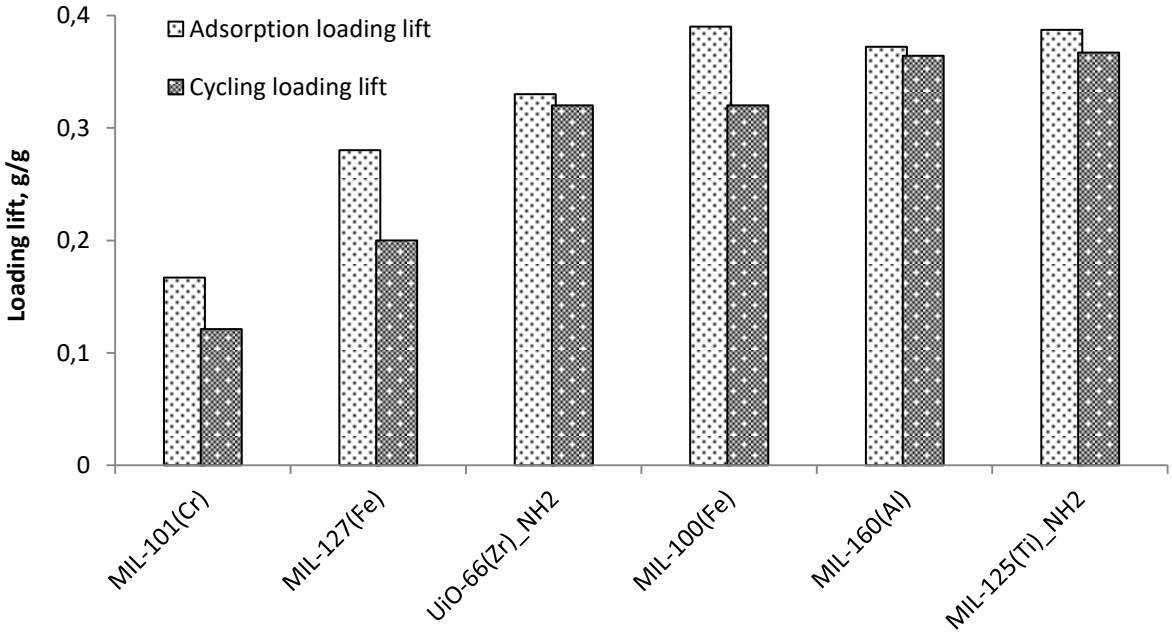

Figure S20. Adsorption and cycling loading lifts of MOFs. Cycle conditions: adsorption at 30°C and 12.5 mbar and desorption at 80°C and 12.5 mbar. Adsorption condition: 30°C and 12.5 mbar

Further we will provide water sorption tests of MOFs using one of these techniques: TG-DSC coupled to humidity generator or IGASorp. The mass profile (Δm) under cycling conditions (adsorption at 30°C, desorption at 80°C, p=12.5 mbar) is presented in absolute units (mg of exchanged water).

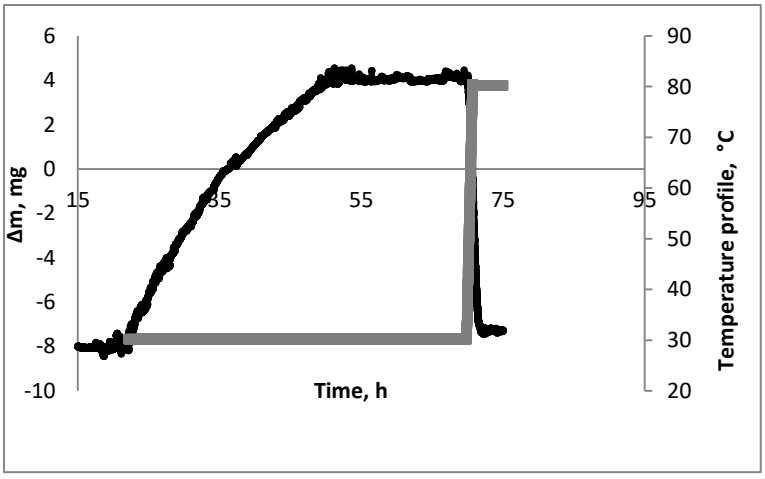

Figure S21. Mass profile (TG-DSC) for MIL-125(Ti)-NH_2 under cycling conditions (on 30.90 mg of anhydrous sample).

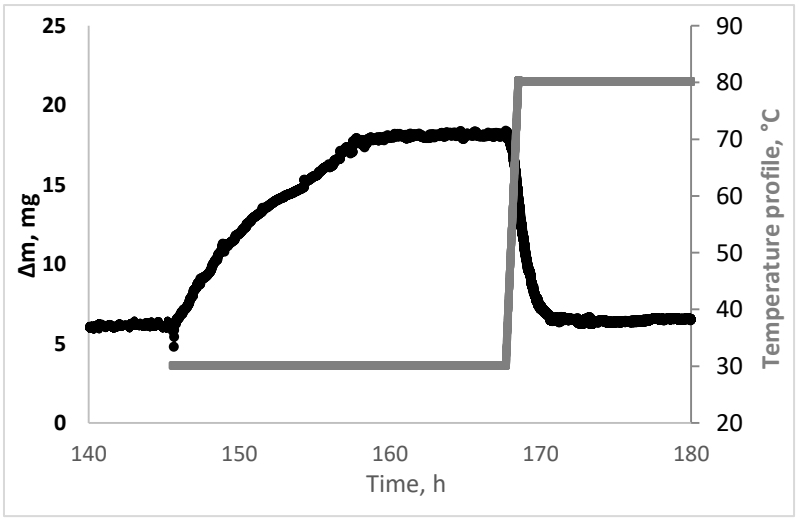

Figure S22. Mass profile (TG-DSC) for MIL-160(Al) under cycling conditions (on 31.83 mg of anhydrous sample).

Figure S23. Mass profile (TG-DSC) for UiO-66(Zr)-NH_2 under cycling conditions (on 33.10 mg of anhydrous sample).

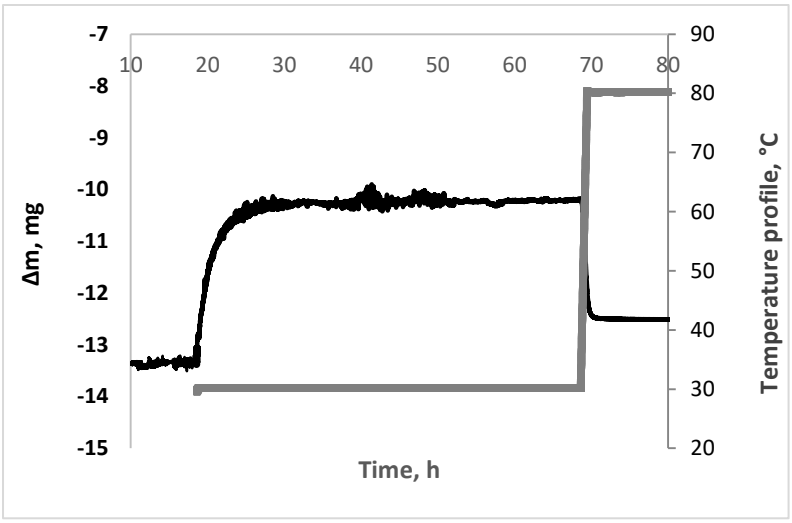

Figure S24. Mass profile (TG-DSC) for MIL-101(Cr) under cycling conditions (on 19.00 mg of anhydrous sample).

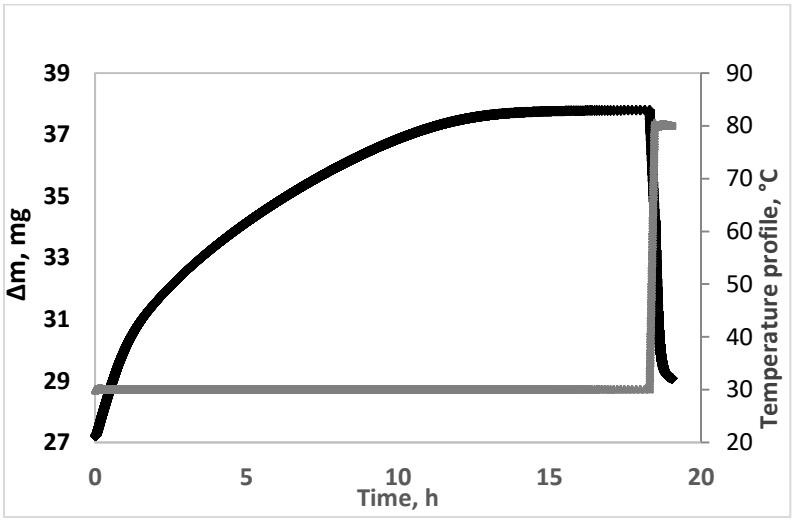

Figure S25. Mass profile (IGASorp) for MIL-100(Fe) under cycling conditions (on 27.21 mg of anhydrous sample).

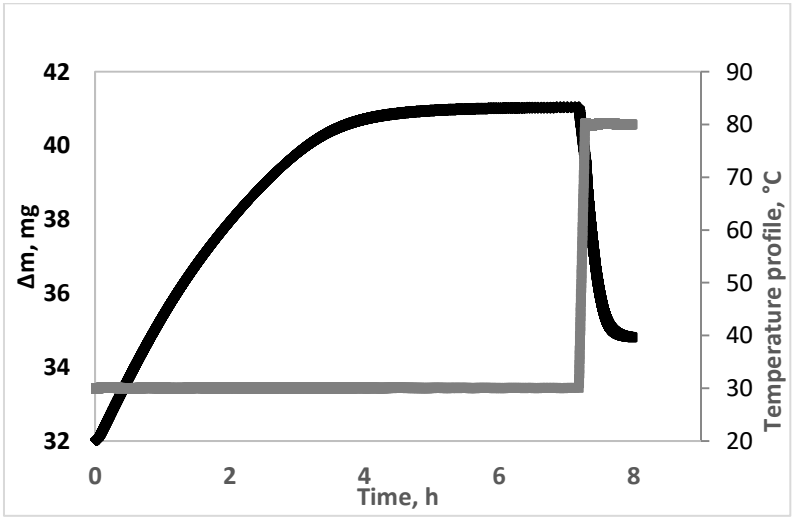

Figure S26. Mass profile (IGASorp) for MIL-127(Fe) under cycling conditions (on 32.04 mg of anhydrous sample).

IV. Synthesis and Characterization of salt-MOF composites

1. Synthesis of salt-MOF composites

The detailed preparation process includes soaking MOFs in inorganic salt solution and drying afterwards. Several parameters of the preparation condition, including concentration of the inorganic salt solution, the volume of inorganic salt solution used for soaking, soaking time, soaking temperature, cycles of soaking, drying temperature were investigated in order to achieve the optimal sample with controlled salt content, good stability and reproducibility. We provide herein the details of composite synthesis indicated in Table S1.
MOF sample was dried for 3 hours in an oven at 100 °C, before one encapsulation step using $CaCl_2$ solution with soaking time of 2 hours. The sample was collected following the removal of excessive $CaCl_2$ solution by centrifugation and was completely dried at 100 ºC in an oven for overnight.

Table S1. Synthesis of salt-MOF composites

Name of composite	MOF-matrix	m of MOF sample, (mg)	V of salt solution (ml)	Concentration of salt solution (%)
MIL-100/$CaCl_2$ (46% wt.)	MIL-100(Fe)	200	0.8	35
MIL-100/$CaCl_2$ (34% wt.)	MIL-100(Fe)	200	0.8	25
MIL-127/$CaCl_2$ (31% wt.)	MIL-127(Fe)	200	0.8	20
MIL-127/$CaCl_2$ (40% wt.)	MIL-127(Fe)	200	0.8	30
UiO-66-NH_2/$CaCl_2$ (43% wt.)	UiO-66(Zr)-NH_2	80	0.8	40
MIL-125(Ti)-NH_2/$CaCl_2$ (45% wt.)	MIL-125(Ti)-NH_2	80	0.8	30
MIL-101(Cr)/CaCl2 (62%)	MIL-101(Cr)	200	0.8	28
MIL-160/$CaCl_2$ (34%)	MIL-160(Al)	80	0.8	40

2. X-ray powder diffraction of composites

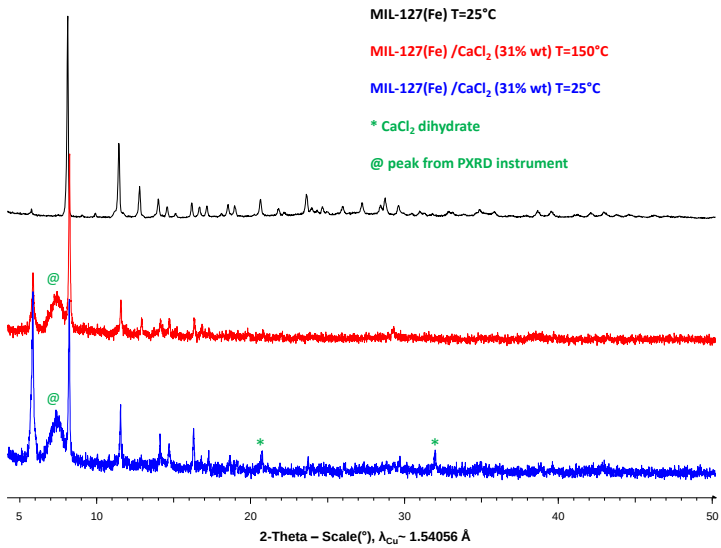

Figure S27. PXRD patterns of MIL-127(Fe) and composite MIL-127(Fe)/$CaCl_2$ (31% wt).

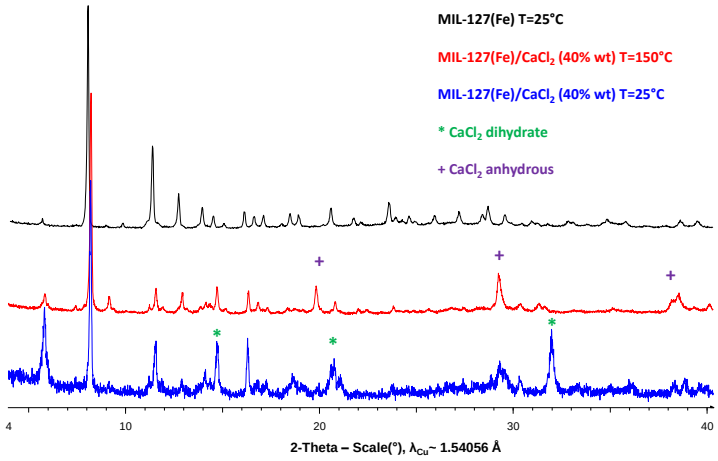

Figure S28. PXRD patterns of MIL-127(Fe) and composite MIL-127(Fe)/$CaCl_2$ (40% wt).

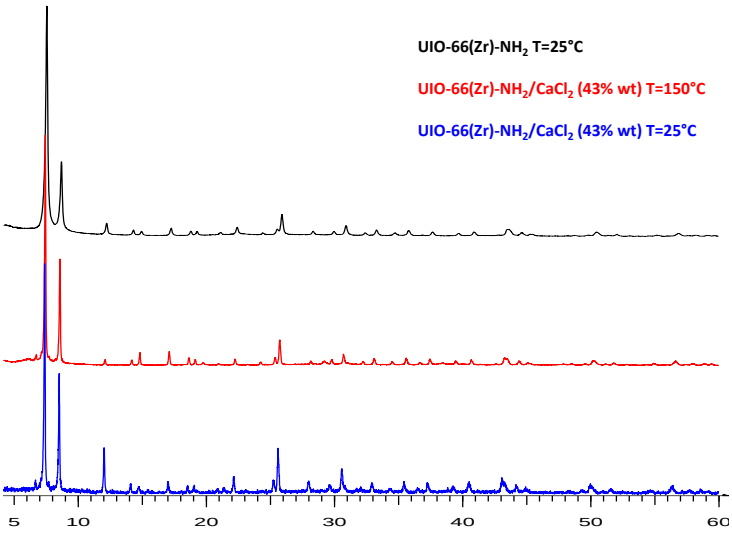

Figure S29. PXRD patterns of UIO-66(Zr)-NH_2 and composite UIO-66(Zr)-NH_2/$CaCl_2$ (43 %).

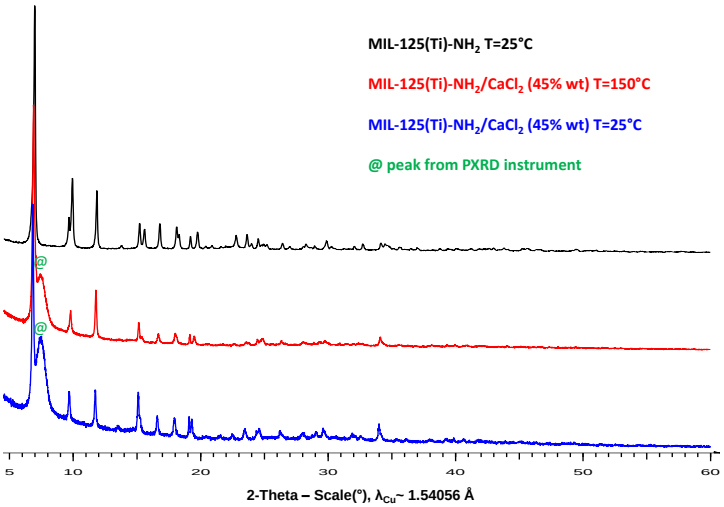

Figure S30. PXRD patterns of MIL-125(Ti)-NH_2 and composite MIL-125(Ti)-NH_2/$CaCl_2$ (45 %).

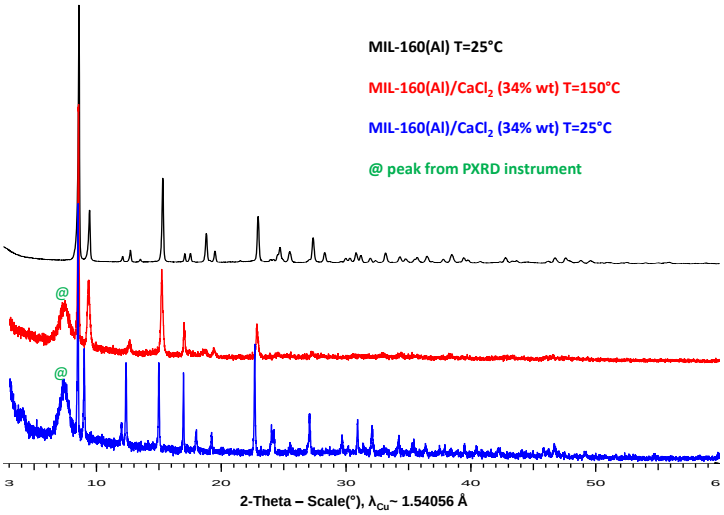

Figure S31. PXRD patterns of MIL-160(Al) and composite MIL-160(Al)/$CaCl_2$ (34 %).

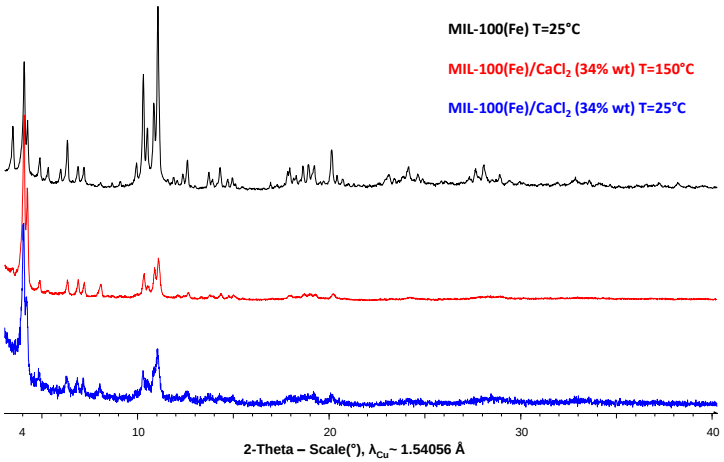

Figure S32. PXRD patterns of MIL-100(Fe) and composite MIL-100(Fe)/$CaCl_2$ (34% wt).

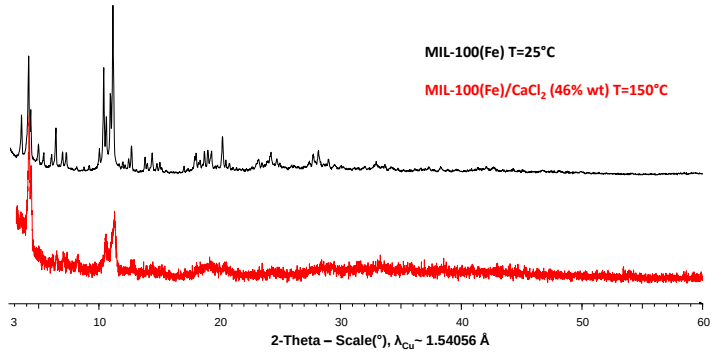

Figure S33. PXRD patterns of MIL-100(Fe) and composite MIL-100(Fe)/$CaCl_2$ (46% wt).

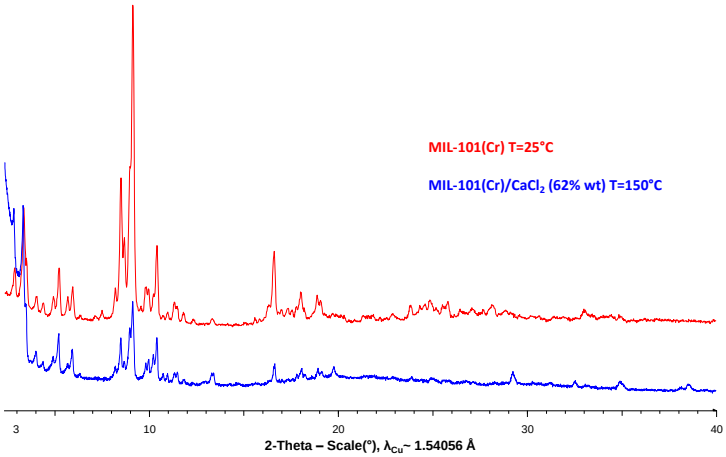

Figure S34. PXRD patterns of MIL-101(Cr) and composite MIL-101(Cr)/$CaCl_2$ (62% wt).

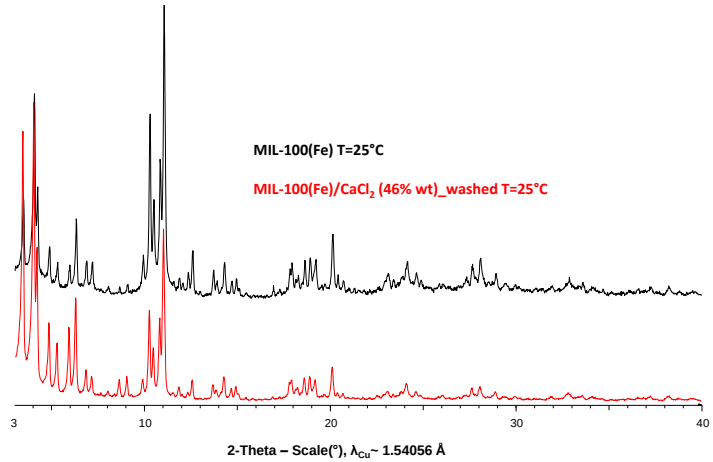

Figure S35. PXRD patterns of MIL-100(Fe) and composite MIL-100(Fe)/$CaCl_2$ (46% wt) after washing

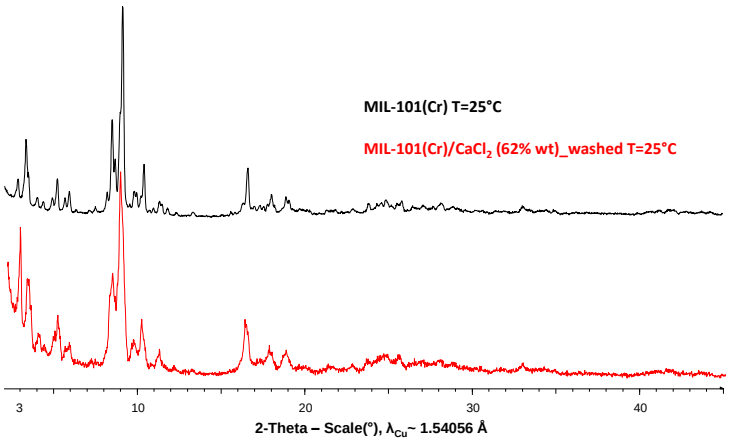

Figure S36. PXRD patterns of MIL-101(Cr) and composite MIL-101(Cr)/$CaCl_2$ (62% wt) after washing

3. Calculation of the salt content

Thermogravimetric analysis

For each composite, three identical samples prepared with the same synthesis conditions were considered and the chemical composition of $CaCl_2$-MOFs composites given in Table S1 is the average of that of the three samples. Thermogravimetric analysis of composites was performed in order to estimate the $CaCl_2$ content and thermal stability of composites. Thermogravimetric profile of composite consists of two weight losses. The first

one between 25°C and 260°C corresponds to water departure. The second continuous weight loss from 260 to 600°C can be assigned to the departure of the organic ligand. Taking into account the melting point of $CaCl_2$ at 773 °C we can consider that metal oxide (Fe_2O_3, Cr_2O_3, TiO_2, ZrO_2, Al_2O_3) and $CaCl_2$ are presented in the mixture at T=600°C. According to the molar amount of the organic and inorganic moiety for each MOF it is possible to extract the amount of $CaCl_2$ in composite considering that the inorganic part of composite at T=600°C is a mixture of metal oxide from each MOF and $CaCl_2$. It can be presented as follow:

$$\boldsymbol{\omega_{salt} = x_{inorg} - \frac{x_{org}}{R}}$$

Here $\boldsymbol{\omega_{salt}}$ is the salt content of anhydrous composite, x_{inorg} is the content of inorganic mixture in the anhydrous composite calculated from thermogravimetric analysis of composite at T=600°C, x_{org} is the content of organic moiety in the anhydrous composite calculated from thermogravimetric analysis of composite, and R is the organic/inorganic ratio of anhydrous MOF calculated from thermogravimetric profile of MOF.

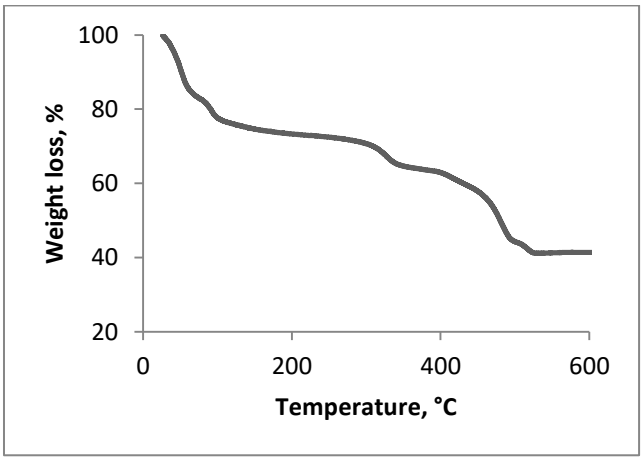

Figure S37. Thermogravimetric analysis profile of MIL-127(Fe)/$CaCl_2$ (40% wt.) under oxygen flow (carrier gas flow rate: 200 ml/min).

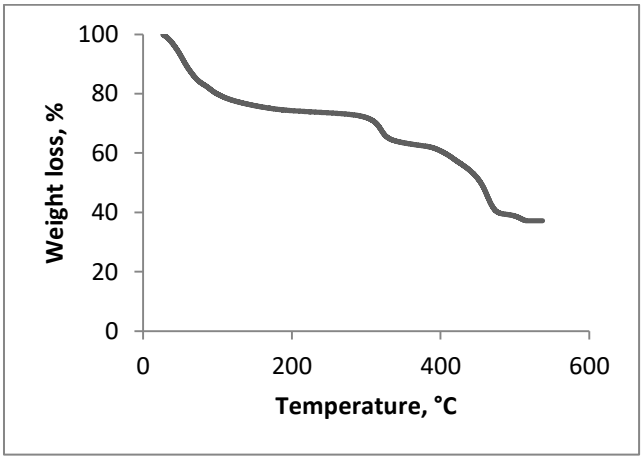

Figure S38. Thermogravimetric analysis profile of MIL-127(Fe)/$CaCl_2$ (31% wt.) under oxygen flow (carrier gas flow rate: 200 ml/min).

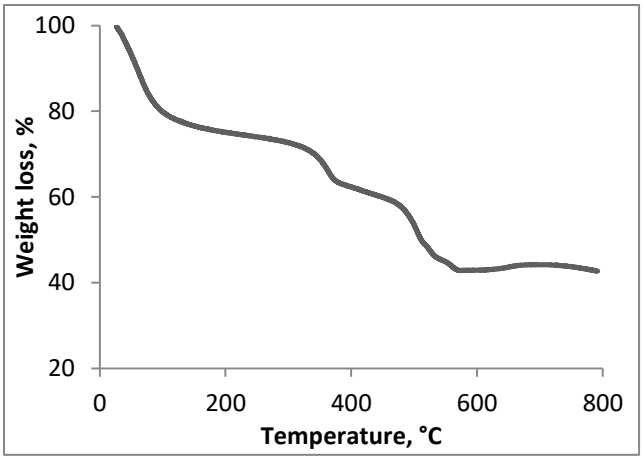

Figure S39. Thermogravimetric analysis profile of MIL-100(Fe)/$CaCl_2$ (34% wt.) under oxygen flow (carrier gas flow rate: 200 ml/min).

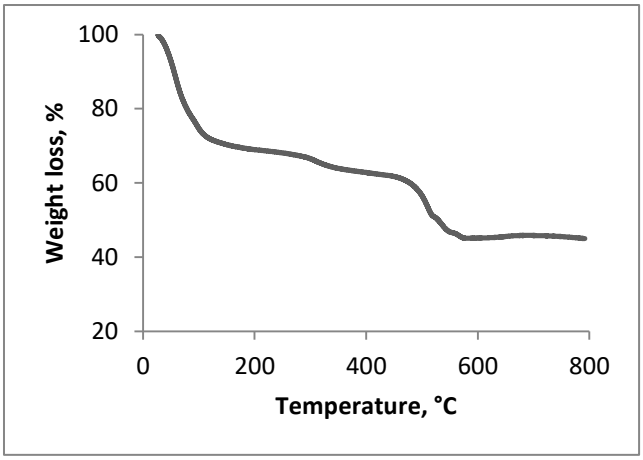

Figure S40. Thermogravimetric analysis profile of MIL-100(Fe)/$CaCl_2$ (46 % wt.) under oxygen flow (carrier gas flow rate: 200 ml/min).

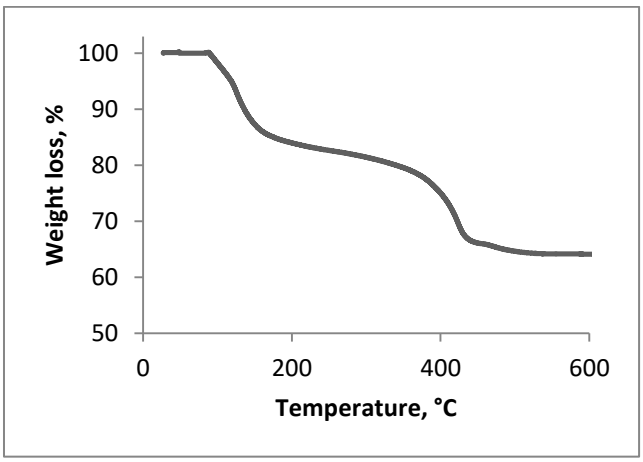

Figure S41. Thermogravimetric analysis profile of MIL-101(Cr)/$CaCl_2$ (62 % wt.) under oxygen flow (carrier gas flow rate: 200 ml/min).

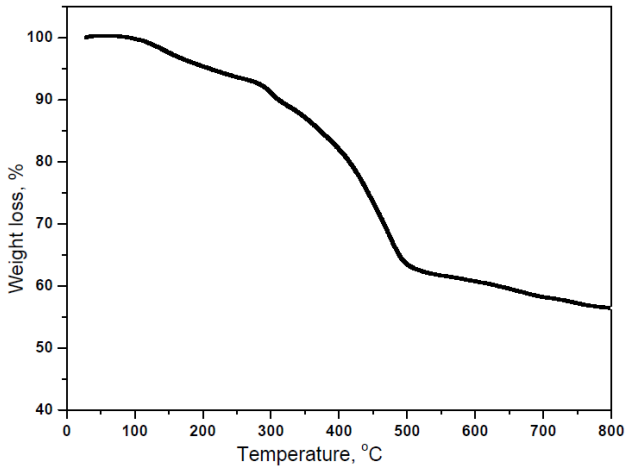

Figure S42. Thermogravimetric analysis profile of MIL-125(Ti)-NH_2/$CaCl_2$ (45% wt.) under oxygen flow (carrier gas flow rate: 200 ml/min).

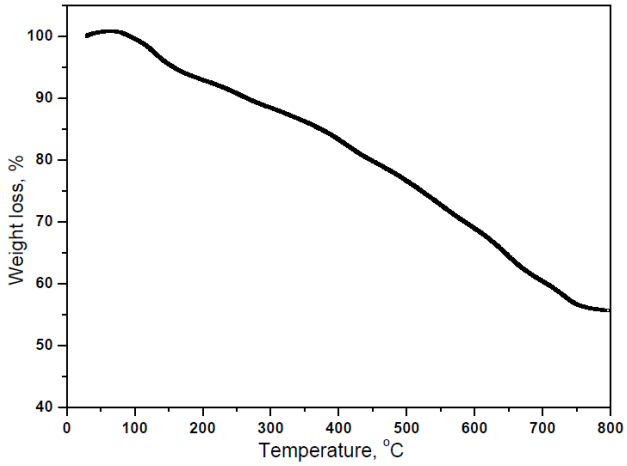

Figure S43. Thermogravimetric analysis profile of UIO-66(Zr)-NH_2/$CaCl_2$ (43% wt.) under oxygen flow (carrier gas flow rate: 200 ml/min).

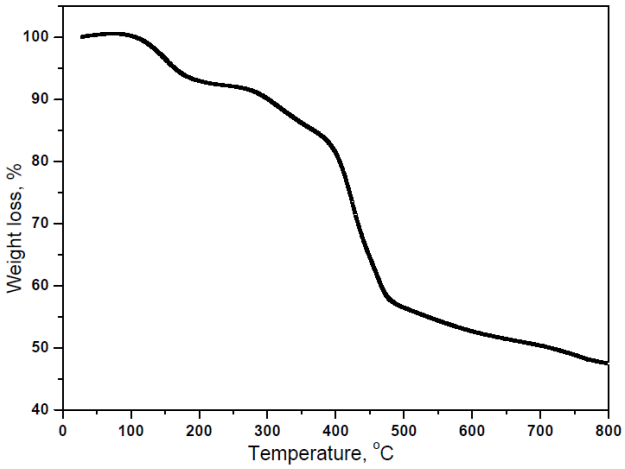

Figure S44. Thermogravimetric analysis profile of MIL-160(Al)/$CaCl_2$ (34% wt.) under oxygen flow (carrier gas flow rate: 200 ml/min).

Elemental analysis of composites

Salt content in composites was calculated twice. The first estimation considers only Ca/Metal (Ca/Me) ratio from elemental analysis (considering molar ratio Cl/Ca equal 2 according to the salt formula as $CaCl_2$). This salt content mentioned in the Table S2 as ω_{CaCl2} (Ca/Me ratio) was compared with salt content obtained by TGA. The second salt content labeled as $\omega_{(Ca+Cl)}$ (Ca/Me and Cl/Fe ratio) takes into account the content of Ca^{2+} and Cl^-

in the composite given by elemental analysis. For all composites, the Cl/Ca ratio is lower than 2 showing a lack of Cl in comparison to the stoichiometry of $CaCl_2$. Finally, we considered the salt content given by $\omega_{(Ca+Cl)}$ (see table S2).

SEM-XEDS of composites

SEM and XEDS analysis were carried out for 3 areas of each composite. SEM analysis shows that the size and shape of MOF crystallite is not affected upon salt encapsulation. The repartition of Me, Ca, Cl elements given by EDS mapping for all composites is quite homogeneous. No $CaCl_2$ crystallites could be observed on SEM images. These results suggest that Ca and Cl elements are distributed inside the pores of MOF matrix.

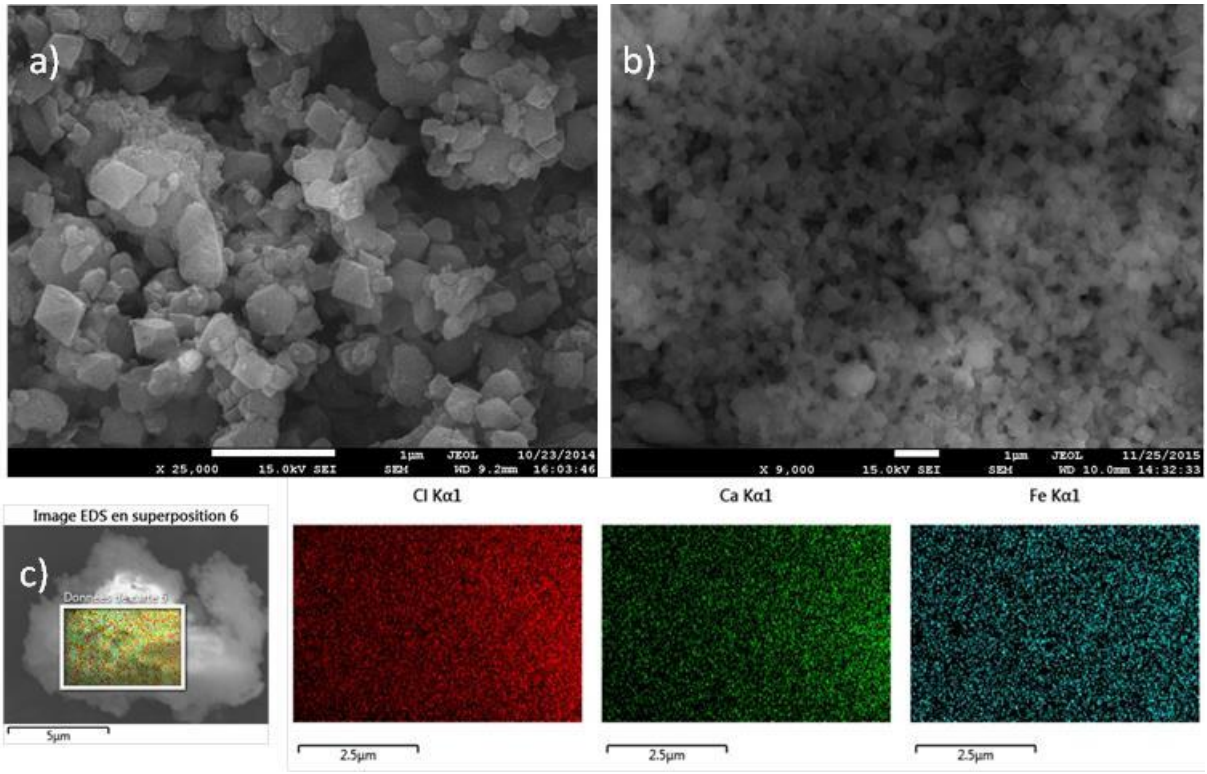

Figure S45. a) SEM of MIL-100(Fe); b) SEM of MIL-100(Fe)/$CaCl_2$ (46%); c) EDS mapping area images for the MIL-100(Fe)/$CaCl_2$ (46%)

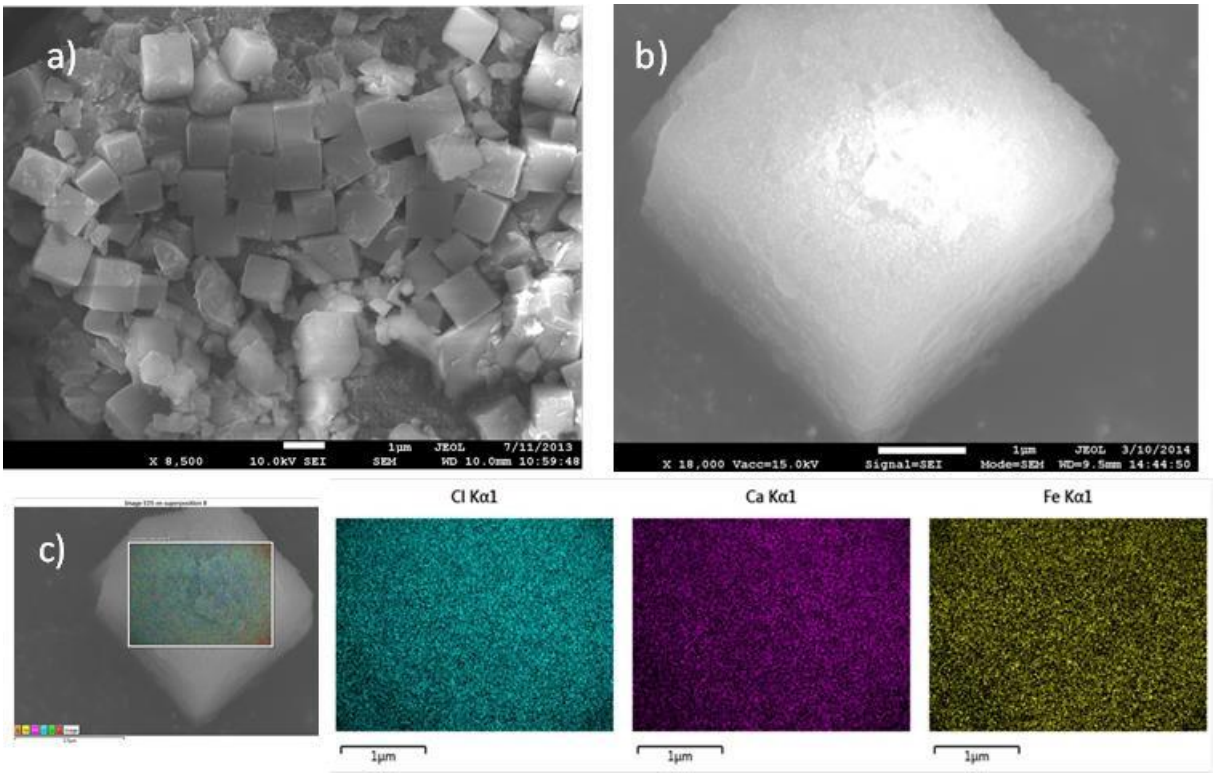

Figure S46. a) SEM of MIL-127(Fe); b) SEM of MIL-127(Fe)/$CaCl_2$ (40%); c) EDS mapping area images for the MIL-127(Fe)/$CaCl_2$ (40%)

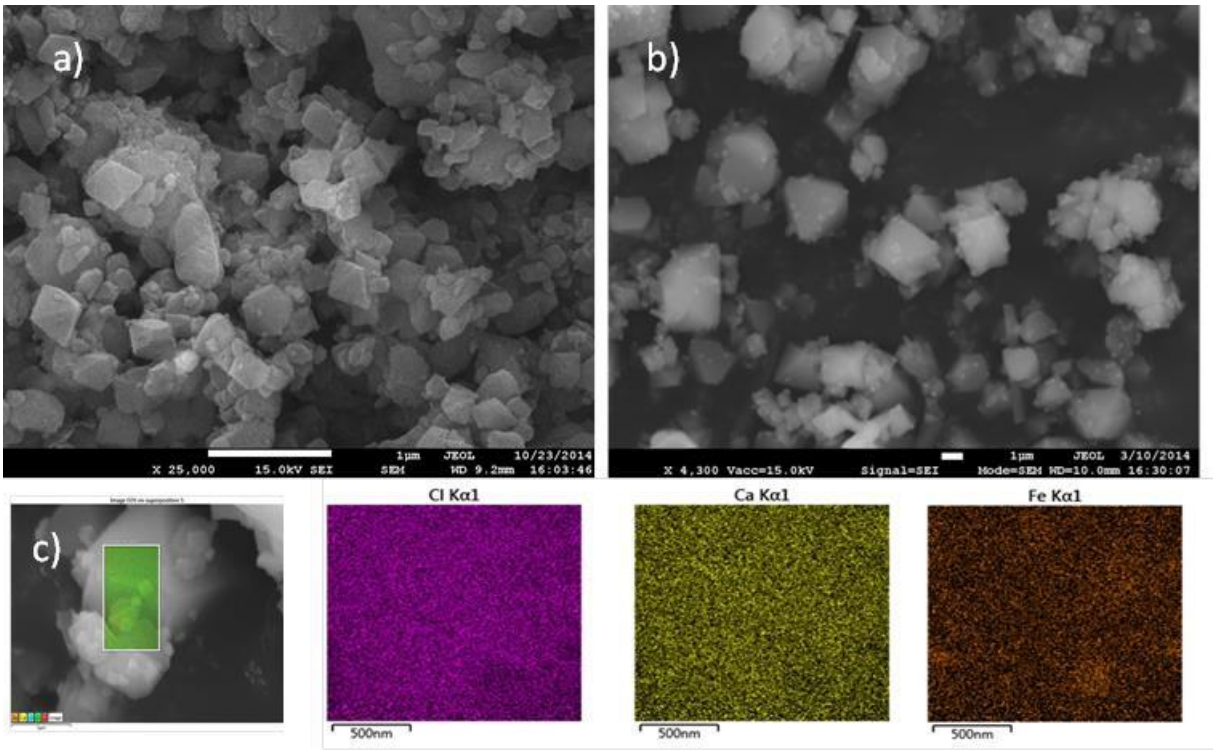

Figure S47. a) SEM of MIL-100(Fe); b) SEM of MIL-100(Fe)/$CaCl_2$ (34%); c) EDS mapping area images for the MIL-100(Fe)/$CaCl_2$ (34%)

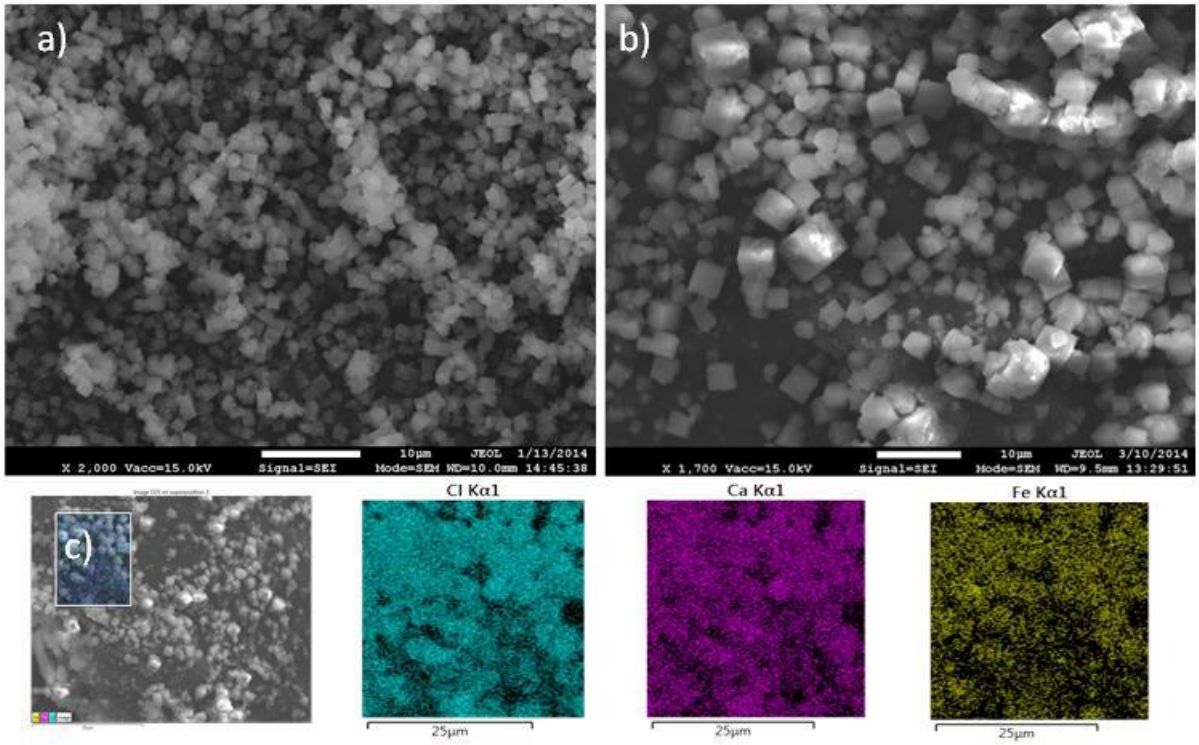

Figure S48. a) SEM of MIL-127(Fe); b) SEM of MIL-127(Fe)/$CaCl_2$ (31%); c) EDS mapping area images for the MIL-127(Fe)/$CaCl_2$ (31%)

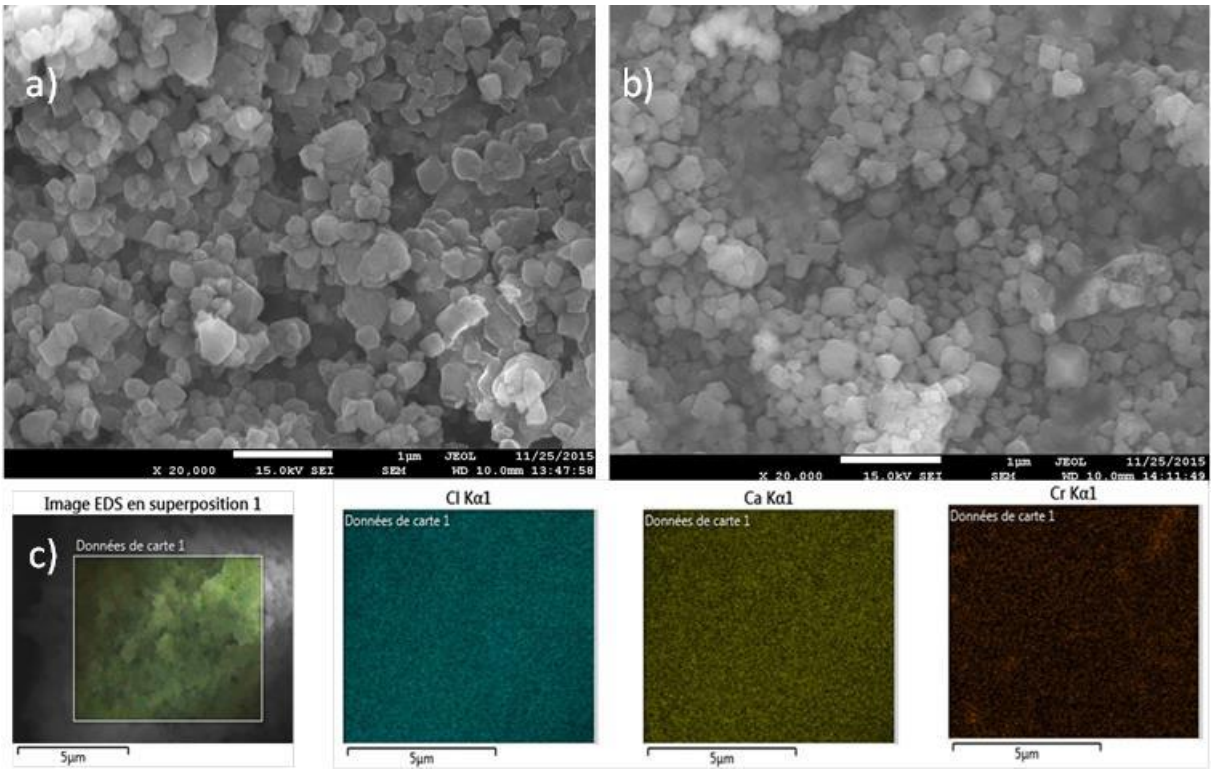

Figure S49. a) SEM of MIL-101(Cr); b) SEM of MIL-101(Cr)/$CaCl_2$ (62%); c) EDS mapping area images for the MIL-101(Cr)/$CaCl_2$ (62%)

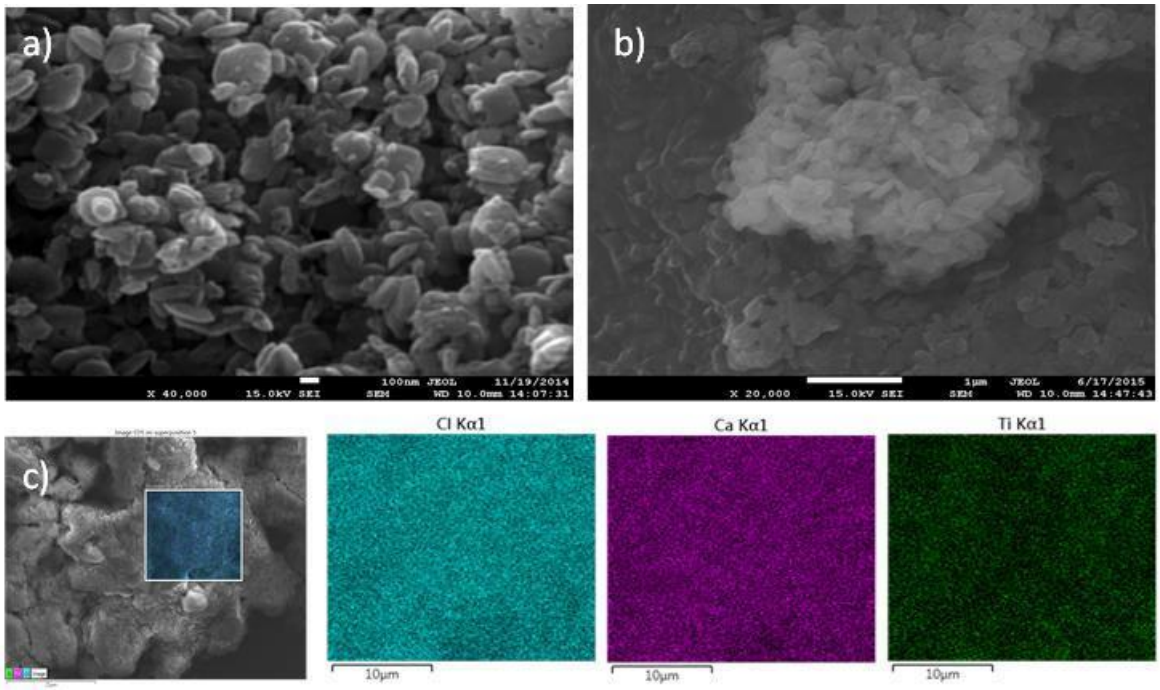

Figure S50. a) SEM of MIL-125(Ti)-NH_2**;** b) SEM of MIL-125(Ti)-NH_2/$CaCl_2$ (45%); c) EDS mapping area images for the MIL-125(Ti)-NH_2/$CaCl_2$ (45%)

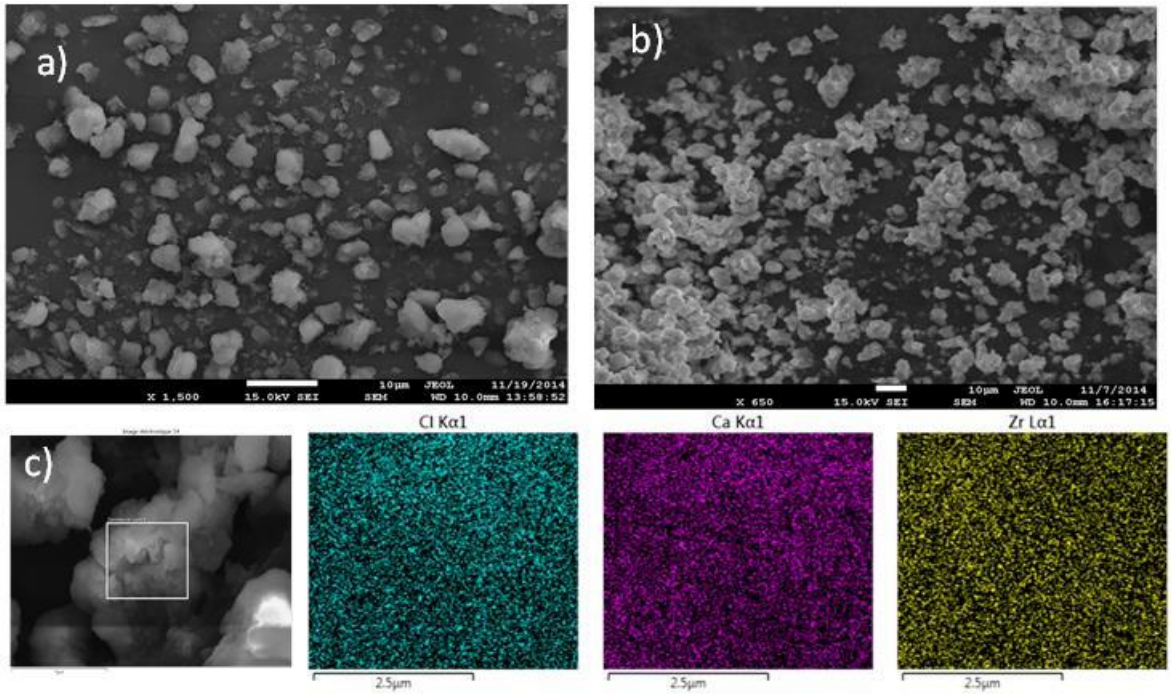

Figure S51. a) SEM of UIO-66(Zr)-NH_2; b) SEM of UIO-66(Zr)-NH_2/$CaCl_2$ **(**43%); c) EDS mapping area images for the UIO-66(Zr)-NH_2/$CaCl_2$ (43%)

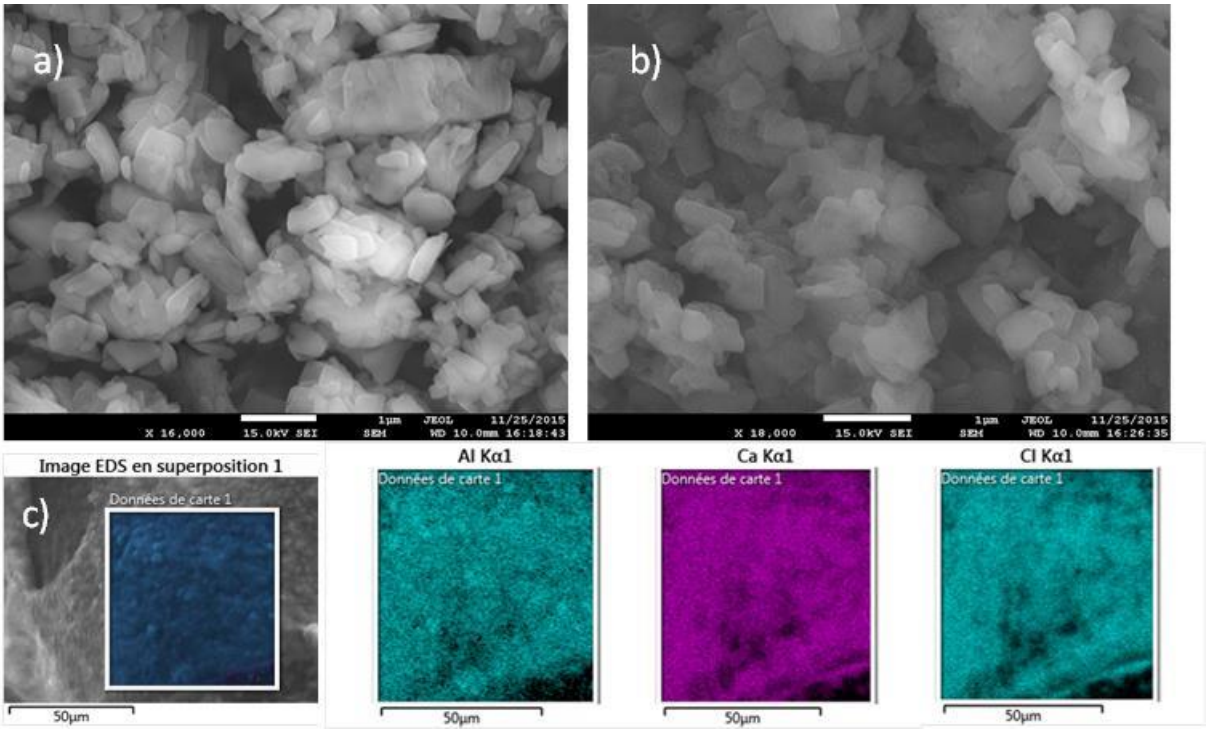

Figure S52. SEM of MIL-160(Al)**;** b) SEM of MIL-160(Al)//$CaCl_2$ (34%); c) EDS mapping area images for the MIL-160(Al)/$CaCl_2$ (34%)

Salt content of composites calculated by thermogravimetry,* X*EDS and elemental analysis (EA)

Table S2. Salt content in composites calculated from thermogravimetry, Ca/Me XEDS ratio and elemental analysis (EA) (based on Ca/Me ratio and based on both Ca/Me and Cl/Me ratio).

Name of composite	ω $CaCl_2$ (TGA) (% wt.)	Ca/Me (XEDS)	Ca/Me (EA)	Cl/Ca (EA)	ω $CaCl_2$ (Ca/Me ratio) (XEDS) (% wt.)	ω $CaCl_2$ (Ca/Me ratio) (EA) (% wt.)	ω (Ca + Cl) (Ca/Me and Cl/Me) (elem. analysis) (% wt.)
MIL-100(Fe)/$CaCl_2$ (**46 wt%**)	48	1.7±0.1	1.96	1.54	48±1	50	**46**
MIL-100(Fe)/$CaCl_2$ (**34 wt%**)	36	0.9±0.2	1.17	1.49	33±5	37	**34**
MIL-127(Fe)/$CaCl_2$ (**31 wt%**)	30	1.4±0.2	1.12	1.69	39±3	34	**31**
MIL-127(Fe)/$CaCl_2$ (**40 wt%**)	39	1.8±0.1	1.69	1.59	43±3	42	**40**
UiO-66(Zr)-NH_2/$CaCl_2$(**43 wt%**)	-	2.0±0.6	2.12	1.82	43±6	44	**43**
MIL-125(Ti)-NH_2/$CaCl_2$ (**45 wt%**)	-	2.3±0.5	1.72	1.70	55±5	48	**45**
MIL-101(Cr)/ $CaCl_2$ (**62 wt%**)	63	2.9±0.2	3.60	1.83	59±2	64	**62**
MIL-160(Al)/$CaCl_2$ (**34 wt%**)	31	1.1±0.3	1.00	1.77	34±3	36	**34**

4. N_2 sorption porosimetry of composites

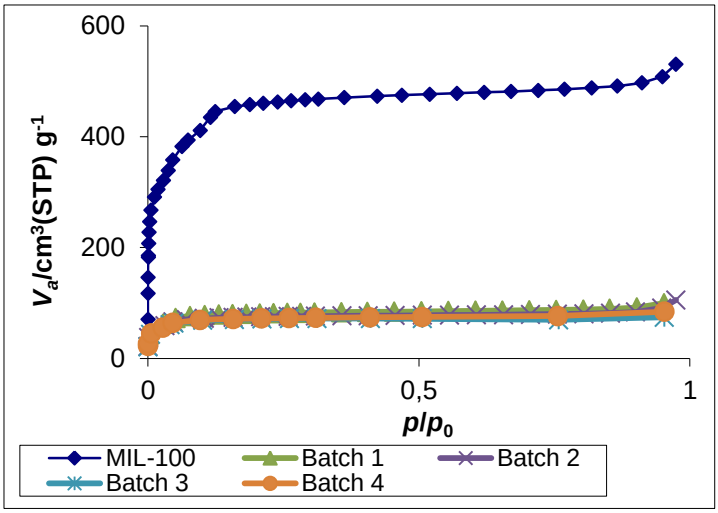

Figure S53. Nitrogen sorption isotherm of MIL-100(Fe) and composite MIL-100(Fe)/$CaCl_2$ (46%) on 4 batches at 77 K. (S_{BET} = 290±20 m^2/g, V_{pore} =0.13±0.02 cm^3/g).

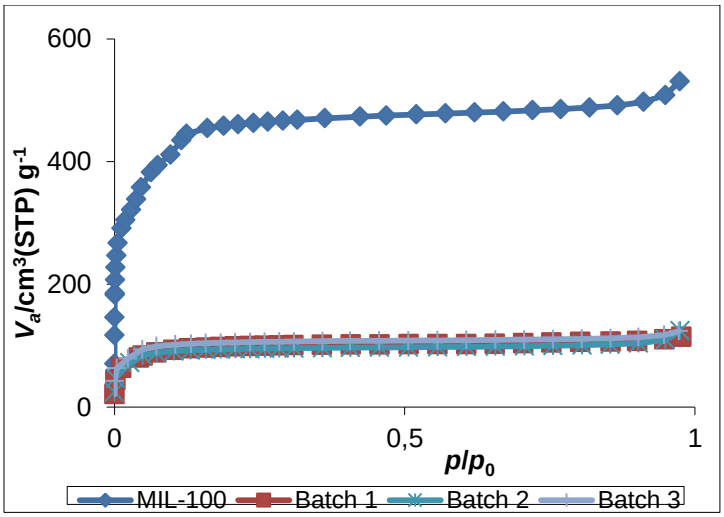

Figure S54. Nitrogen sorption isotherm of MIL-100(Fe) and composite MIL-100(Fe)/$CaCl_2$ (34 %) on 3 batches at 77 K. (S_{BET} = 370±50 m^2/g, V_{pore} =0.188±0.005 cm^3/g).

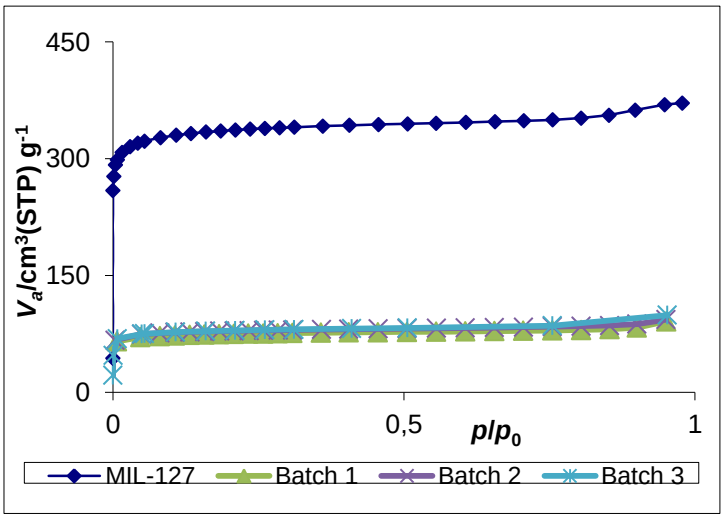

Figure S55. Nitrogen sorption isotherm of MIL-127(Fe) and composite MIL-127(Fe)/$CaCl_2$ (40 %) on 3 batches at 77 K. (S_{BET} = 520±10 m^2/g, V_{pore} =0.223±0.005 cm^3/g).

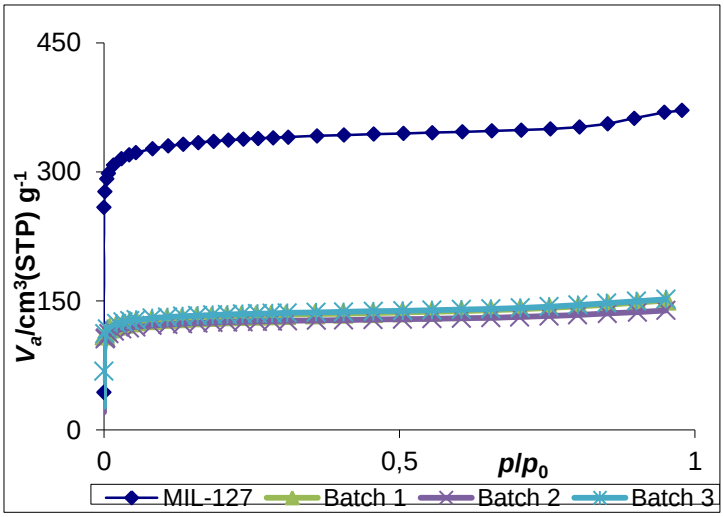

Figure S56. Nitrogen sorption isotherm of MIL-127(Fe) and composite MIL-127(Fe)/$CaCl_2$ (31 %) on 3 batches at 77 K. (S_{BET} = 520±20 m^2/g, V_{pore} =0.228±0.009 cm^3/g).

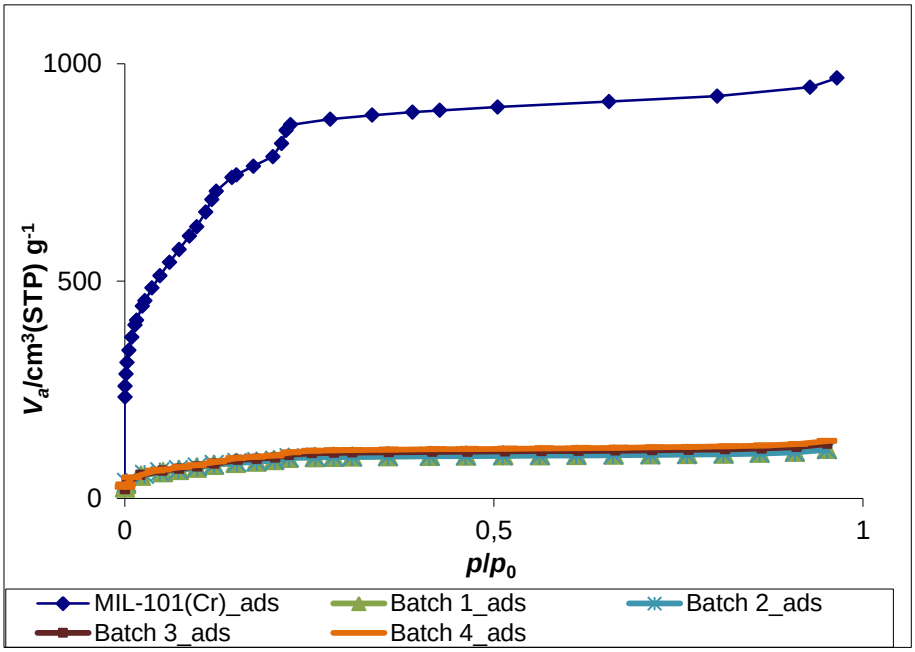

Figure S57. Nitrogen sorption isotherm of MIL-101(Cr) and composite MIL-101(Cr)/$CaCl_2$ (62 %) on 4 batches at 77 K. (S_{BET} = 330±10 m^2/g, V_{pore} =0.19±0.01 cm^3/g).

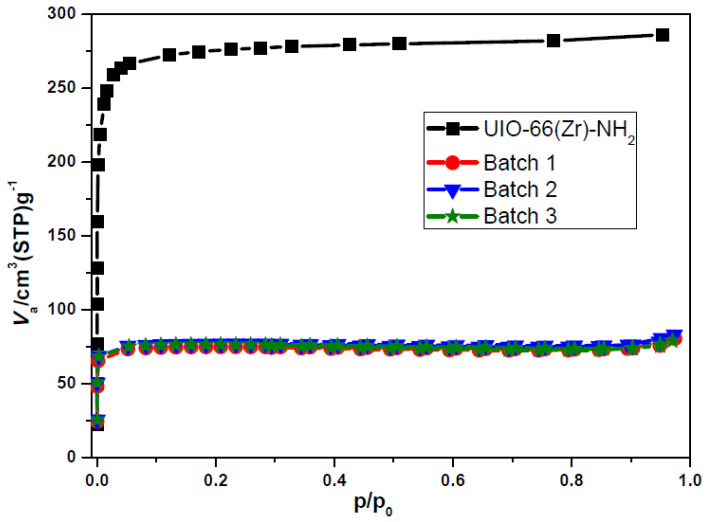

Figure S58. Nitrogen sorption isotherm of UIO-66(Zr)-NH_2 and composite UIO-66(Zr)-NH_2/$CaCl_2$ (43 %) on 3 batches at 77 K. (S_{BET} = 310±10 m^2/g, V_{pore} =0.130±0.004 cm^3/g).

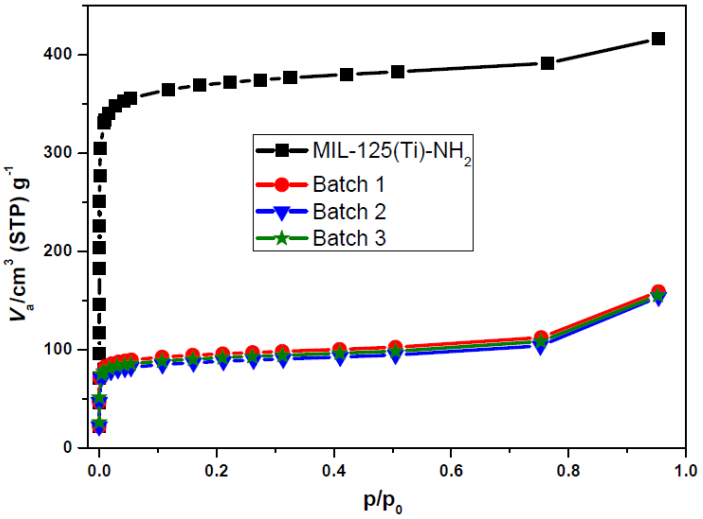

Figure S59. Nitrogen sorption isotherm of MIL-125(Ti)-NH_2 and composite MIL-125(Ti)-NH_2/$CaCl_2$ (45 %) on 3 batches at 77 K. (S_{BET} = 360±20 m^2/g, V_{pore} =0.240±0.004 cm^3/g).

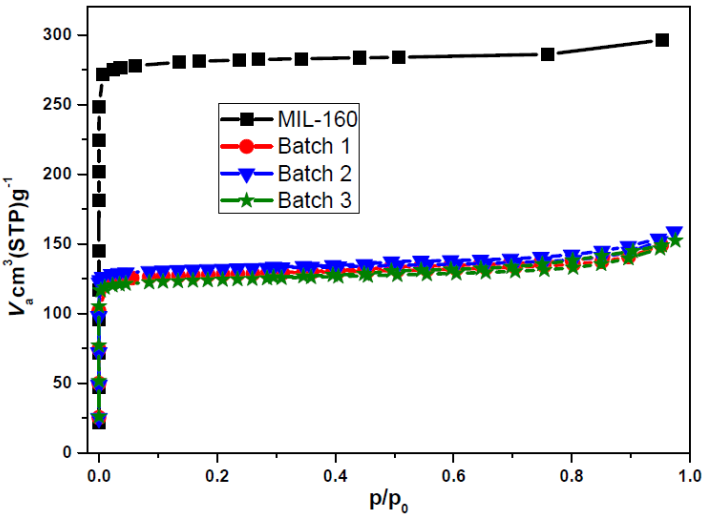

Figure S60. Nitrogen sorption isotherm of MIL-160(Al) and composite MIL-160(Al)/$CaCl_2$ (34 %) on 3 batches at 77 K. (S_{BET} = 520±20 m^2/g, V_{pore} =0.240±0.006 cm^3/g).

5. Water sorption properties of composites. Mass profile under cycling condition

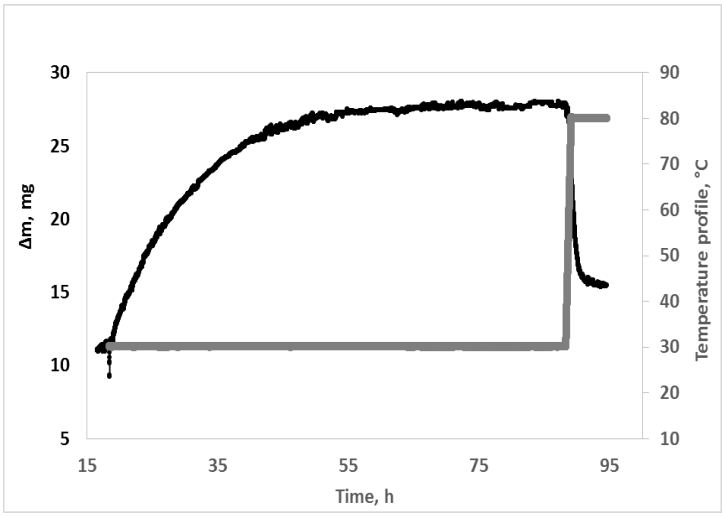

Figure S61. Mass profile (TG-DSC) for MIL-127(Fe)/$CaCl_2$ (40% wt) under cycling conditions (on 36.92 mg of anhydrous sample)

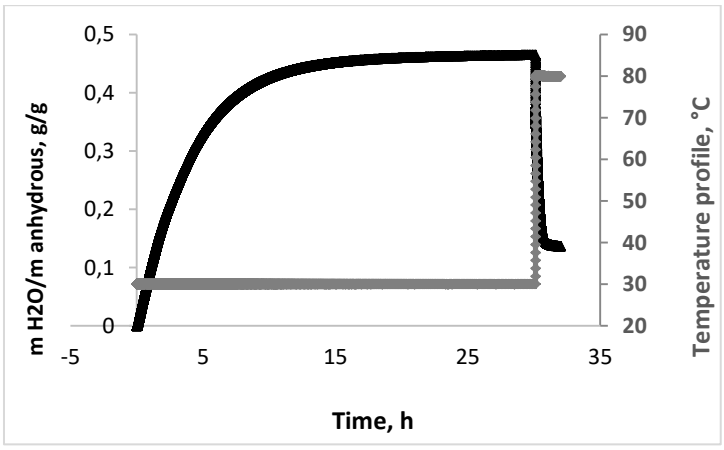

Figure S62. Cycling loading lift (IGASorp) on 28.79 mg of anhydrous MIL-127(Fe)/$CaCl_2$ (31 % wt) composite.

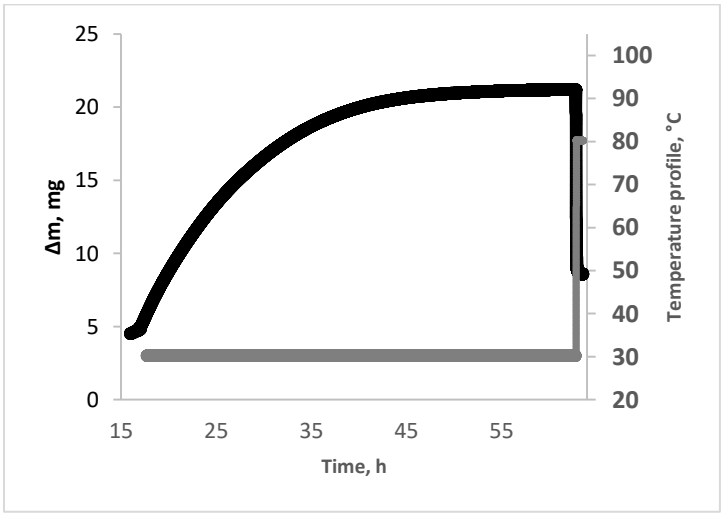

Figure S63. Mass profile (TG-DSC) for MIL-125(Ti)-NH_2/$CaCl_2$ (45% wt.) under cycling conditions (on 35.87 mg of anhydrous sample)

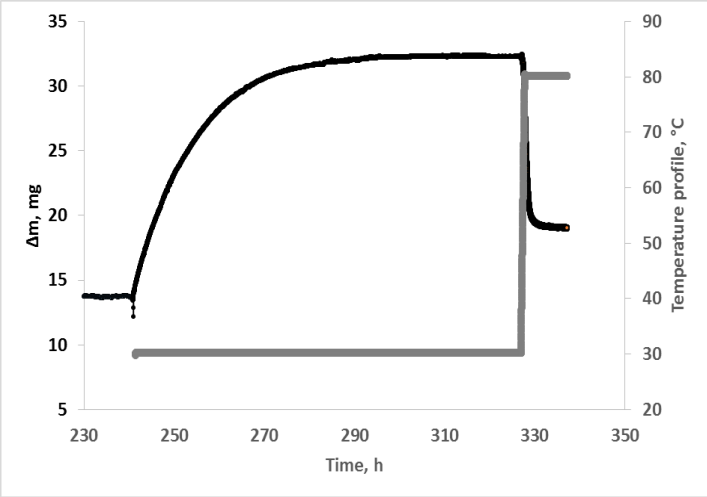

Figure S64. Mass profile (TG-DSC) for UiO-66(Zr)-NH_2/$CaCl_2$ (43% wt.) under cycling conditions (on 39.05 mg of anhydrous sample)

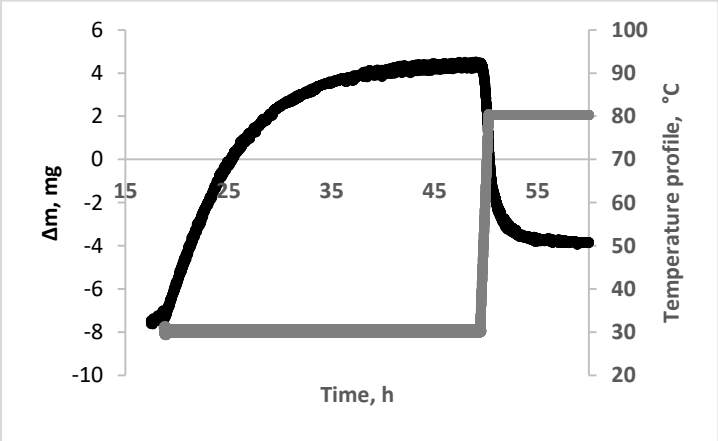

Figure S65. Mass profile (TG-DSC) for MIL-100(Fe)/$CaCl_2$ (34 % wt.) under cycling conditions (on 24.79 mg of anhydrous sample)

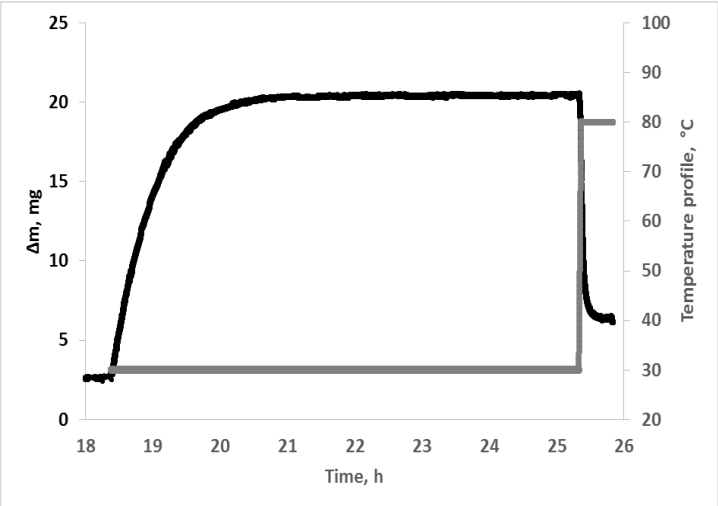

Figure S66. Mass profile (TG-DSC) for MIL-100(Fe)/$CaCl_2$ (46 % wt.) under cycling conditions (on 30.60 mg of anhydrous sample)

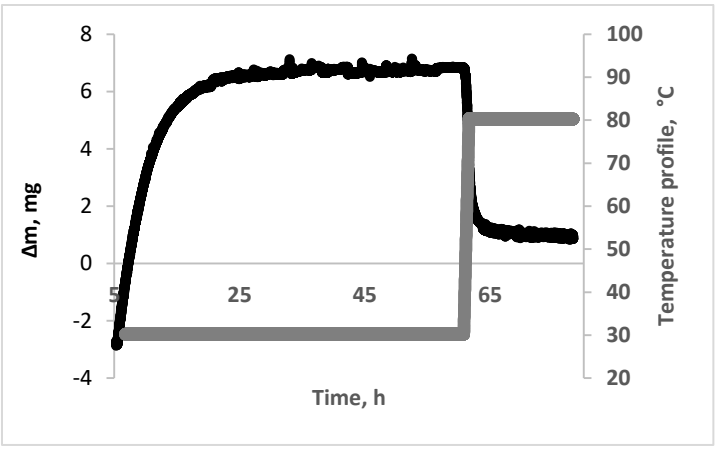

Figure S67. Mass profile (TG-DSC) for MIL-160(Al)/$CaCl_2$ (34 % wt) under cycling conditions (on 27.70 mg of anhydrous sample)

6. Calculation of energy storage capacity and energy storage density

Energy storage density of material corresponds to stored energy per unit of volume [kWh/m^3]. It is a function of three parameters such as differential heat of adsorption, cycle loading lift and packing density of the material. Energy storage capacity of material corresponds to stored energy per unit of mass [Wh/kg] and depends only on differential heat of adsorption and cycle loading lift of material.

We calculated a theoretical energy storage capacity and energy storage density of second series of composites, considering that a part of the hydration is due to the chemical reaction of $CaCl_2$ from monohydrate to hexahydrate and the residual part is due to the physical adsorption on MOF. This calculation requires the heat of hydration and the heat of adsorption in conditions of cycling loading lift. According to phase diagram of $CaCl_2$ three reactions of dehydration take place at p=12.5 mbar between 30 and 80°C.

$$CaCl_2 \cdot 6H_2O = CaCl_2 \cdot 4H_2O + 2H_2O \quad \left(\Delta H_{chem[6\to4]} = 47255 J/mol\right) \tag{1}$$

$$CaCl_2 \cdot 4H_2O = CaCl_2 \cdot 2H_2O + 2H_2O \quad \left(\Delta H_{chem[4\to2]} = 47850 J/mol\right) \tag{2}$$

$$CaCl_2 \cdot 2H_2O = CaCl_2 \cdot 1H_2O + H_2O \quad \left(\Delta H_{chem[2\to1]} = 47557 J/mol\right) \tag{3}$$

The heat of adsorption (ΔH_{phys}) of MOF was measured (see II) according to the condition of cycling loading lift as average integral enthalpy between integral enthalpy corresponding to adsorbed mass and integral enthalpy corresponding to desorbed mass. Thus, energy storage capacity (Q) can be estimated as follow:

$$Q = \Delta m_{chem} \times \Delta H_{chem} + \Delta m_{phys} \times \Delta H_{phys} \tag{4}$$

$$\Delta H_{chem} = \tfrac{1}{5}\Delta H_{chem[2\to1]} + \tfrac{2}{5}\Delta H_{chem[4\to2]} + \tfrac{2}{5}\Delta H_{chem[6\to4]} \tag{5}$$

Here ΔH_{chem} implies enthalpies of above mentioned reaction while Δm_{chem} and Δm_{phys} are exchanged mass corresponding to chemical reaction and physical adsorption, respectively. These exchanged mass can be founded as follow:

$$\Delta m_{chem} = \omega_{chem} \times m_{anhydrous} \tag{6}$$

$$\Delta m_{phys} = \Delta m_{\exp} - \Delta m_{chem} \tag{7}$$

Here $\Delta m_{\exp}$ is total experimental exchanged mass over cycle denoted cycling loading lift.

Energy storage density (E) can be presented as:

$$E = Q \times d \quad (8)$$

where d is packing density of composite material.

We will provide the details of energy storage capacity calculation for second series of composites and energy storage density for composites based on mesoporous MOFs (MIL-100(Fe) and MIL-101(Fe)).

Table S3. Calculated energy storage capacity and energy storage density of second series of composites

Composite	ω (Ca + Cl) from elem. Analysis (% wt.)	Δm_{exp} (g/g)	Δm_{chem} (g/g)	ΔH_{phys} (kJ/mol)	Q calculated (Wh/kg)	d (g/cm^3)	E calculated (kWh/m^3)
MIL-127(Fe)/$CaCl_2$ (40%)	40	0.33	0.324	54.47[a]	243	-	-
MIL-125(Ti)-NH_2/$CaCl_2$ (45%)	45	0.35	0.369	56.45[a]	254	-	-
UiO-66(Zr)-NH_2/$CaCl_2$ (43%)	43	0.33	0.349	52.68[a]	248	-	-
MIL-100(Fe)/$CaCl_2$ (46%)	46	0.47	0.39	49.18[b]	347	0.62	215
MIL-101(Cr)/$CaCl_2$ (62%)	62	0.58	0.50	46.45[b]	428	0.64	274

[a]Heat of adsorption measured in this work; [b]heat of adsorption reported in the literature[1]

7. Measurements of energy storage capacity of second series of composites

The energy storage capacity of the second series of composites was also determined experimentally by measuring the heat of sorption during the desorption step when heating the sample from 30°C to 80°C at 12.5 mbar. This test was done on TG-DSC 111 coupled to Wetsys humidity generator from Setaram. Prior to analysis sample was dried under vacuum at 150°C or 180°C for 10 hours. The sample is then put in contact with humid nitrogen (flow rate: 50 mL/min, bath and gas temperature: 40°C, relative humidity: 17.4%) at 30°C. When the equilibrium is reached, sample is heated to 80°C at 1°C/min, the desorbed mass and the heat flow signals are simultaneously recorded. The desorbed mass between 30°C and 80°C at 12.5 mbar corresponds to the cycle loading lift. The integration of the heat flow signal enables to obtain the heat of sorption, $Q_{measured}$. This value has to be corrected with the integration of the heat flow signal of a blank test (prior to the measurement, blank test is done in the same conditions with empty crucibles), and by taking into account the heat required to heat the sample and the water vapor from 30°C to 80°C.

$$Q_{corrected} = Q_{measured} - Q_{blank} - m_{anhydrous} c_p \Delta T - \Delta m c_{p_w} \Delta T$$

The heat capacity of composite includes that of salt ($CaCl_2$) and corresponding MOF-matrix. In order to take into account the contribution of matrix, the heat capacity of one MOF, namely MIL-100(Fe), was measured experimentally. This value was further used to correct heat capacity contribution of other MOFs in composites.

Table S4. Measured energy storage capacity and energy storage density of second series of composites

Composite	Q corrected (Wh/kg)	d (g/cm^3)	E calculated (kWh/m^3)
MIL-127(Fe)/$CaCl_2$ (40%)	228	-	-
MIL-125(Ti)- NH_2/$CaCl_2$ (45%)	243	-	-
UiO-66(Zr)- NH_2/$CaCl_2$ (43%)	268	-	-
MIL-100(Fe)/$CaCl_2$ (46%)	335	0.62	208
MIL-101(Cr)/$CaCl_2$ (62%)	485	0.64	310

The heat capacity of MIL-100(Fe) was measured on TG-DSC111 coupled to Wetsys humidity generator from Setaram. Prior to analysis a blank test is done with empty crucibles in the same experimental conditions. MIL-100(Fe) is first dried at 180°C during 10 hours under vacuum. A heating treatment is applied to each sample: an isotherm at 20°C is done during 15 minutes, followed by a heating step from 20°C to 180°C at 1°C/min and an isotherm step at 180°C during 15 minutes. The heat capacity is directly calculated by the equipment software. The test is repeated four times.

8. Stability of composites based on MIL-100(Fe) and MIL-101(Cr) upon ageing

8.1. SEM analysis

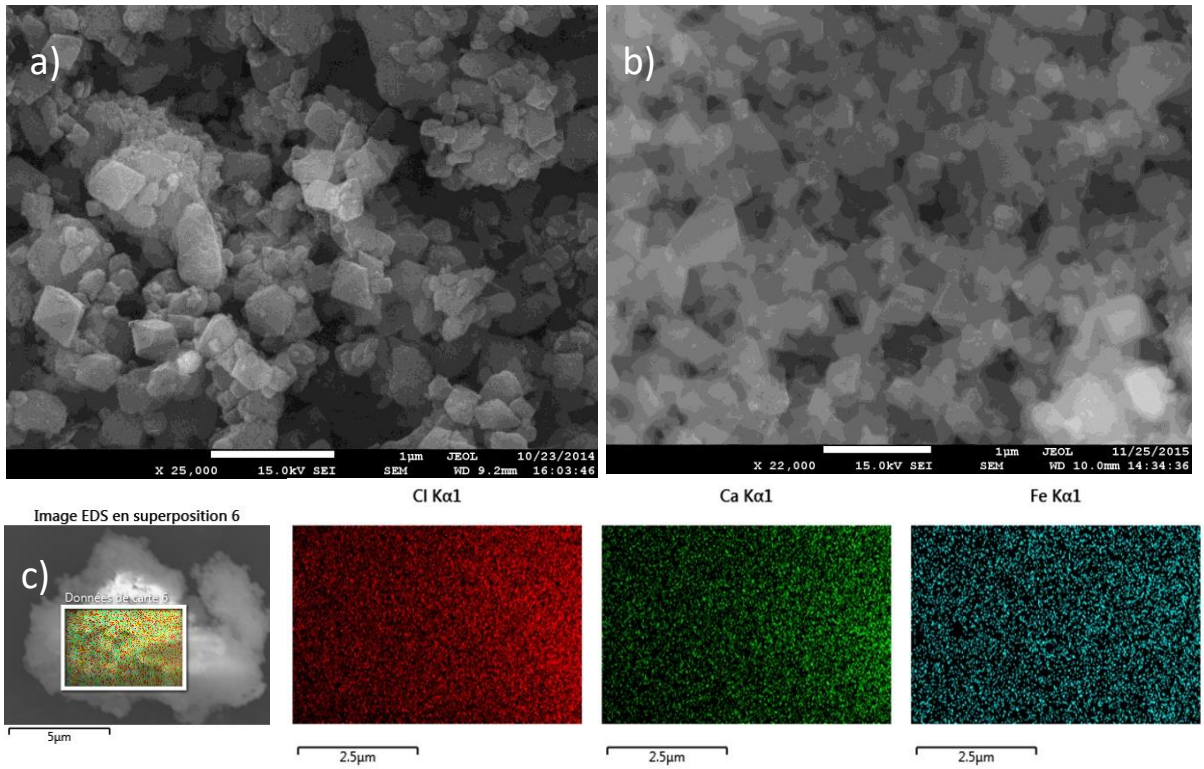

Figure S68. a) SEM of MIL-100(Fe); b) SEM of MIL-100(Fe)/$CaCl_2$ (46%) (1.5 year after synthesis); c) **X**EDS mapping area images for the MIL-100(Fe)/$CaCl_2$ (46%)

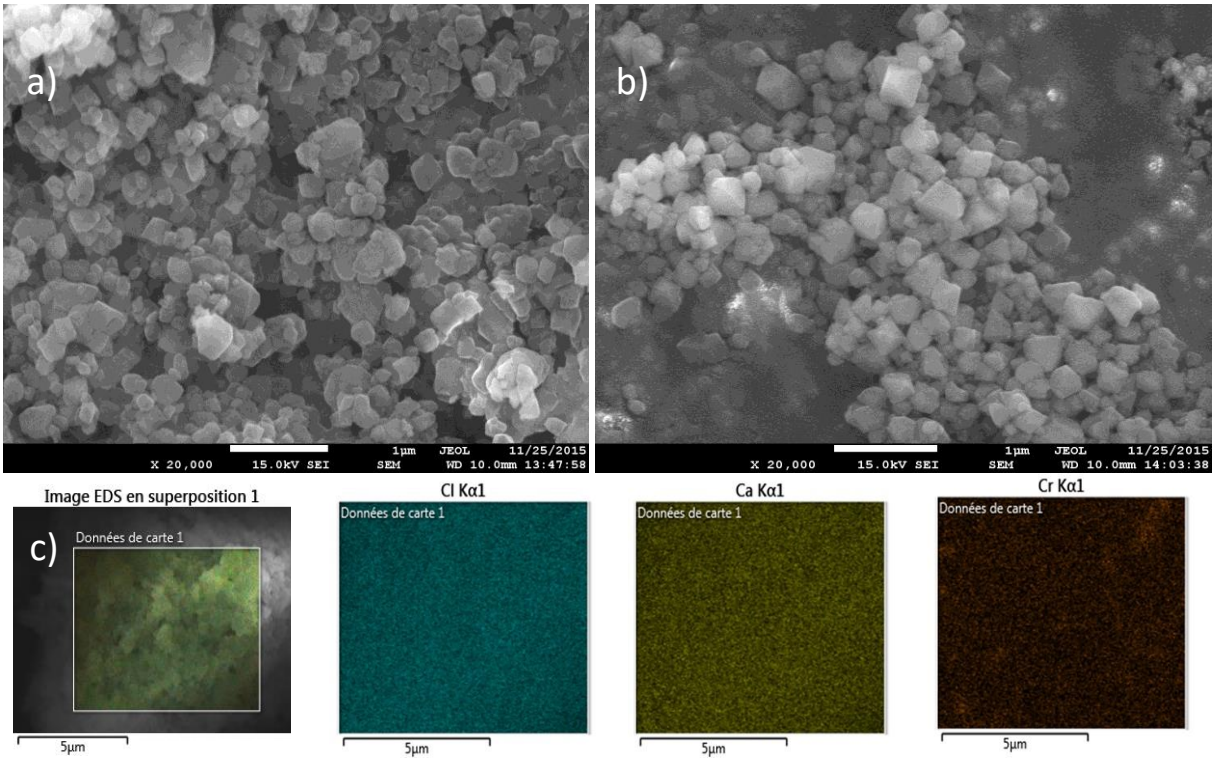

Figure S69. a) SEM of MIL-101(Cr); b) SEM of MIL-101(Cr)/$CaCl_2$ (62%) (0.5 year after synthesis); c) XEDS mapping area images for the MIL-101(Cr)/$CaCl_2$ (62%)

8.2. Nitrogen sorption porosimetry

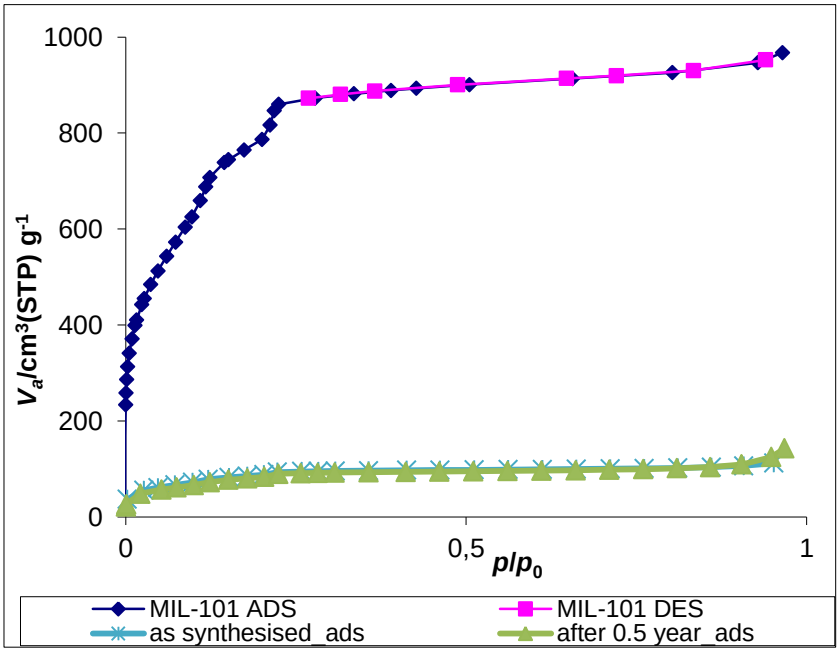

Figure S70. Nitrogen sorption isotherm of MIL-101(Cr) and composite MIL-101(Cr)/$CaCl_2$ (62% wt.) after synthesis (S_{BET} = 323 m^2/g, V_{pore} =0.19 cm^3/g) and after 0.5 years of storing (S_{BET} = 320 m^2/g, V_{pore} =0.22 cm^3/g) at 77 K.

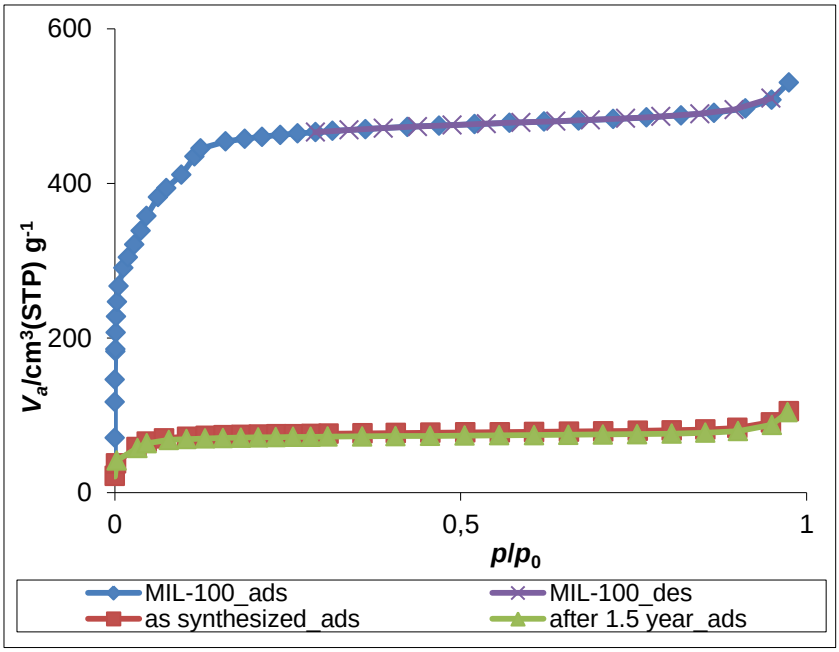

Figure S71. Nitrogen sorption isotherm of MIL-100(Fe) and composite MIL-100(Fe)/$CaCl_2$ (46% wt.) after synthesis (S_{BET} = 278 m^2/g, V_{pore} =0.16 cm^3/g) and after 1.5 years of storing (S_{BET} = 272 m^2/g, V_{pore} =0.16 cm^3/g) at 77 K.

8.3. Thermogravimetric analysis

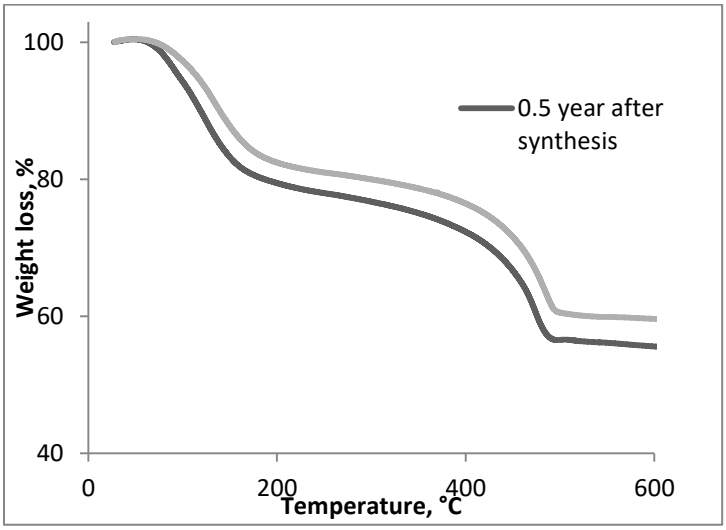

Figure S72. Thermogravimetric analysis profile of MIL-101(Cr)/$CaCl_2$ (62 % wt.) composite under oxygen flow (carrier gas flow rate: 200 ml/min) after synthesis (62 % wt. of $CaCl_2$) and after 0.5 year (60% wt. of $CaCl_2$).

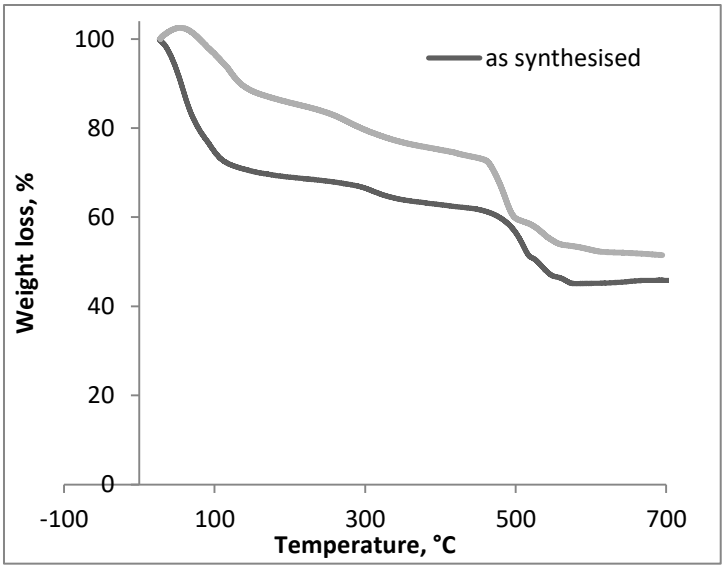

Figure S73. Thermogravimetric analysis profile of MIL-100(Fe)/$CaCl_2$ (46% wt.) composite under oxygen flow (carrier gas flow rate: 200 ml/min) after synthesis (48% wt. of $CaCl_2$) and after 1.5 year (45% wt. of $CaCl_2$).

References:

1 Y.-K. Seo, J. W. Yoon, J. S. Lee, Y. K. Hwang, C.-H. Jun, J.-S. Chang, S. Wuttke, P. Bazin, A. Vimont, M. Daturi, S. Bourrelly, P. L. Llewellyn, P. Horcajada, C. Serre, G. Férey, *Adv. Mater.,* 2012, **24**, 806.